pH Biosensing by PI4P Regulates Cargo Sorting at the TGN

John J.H. Shin[1,2], Peter Liu[1], Leslie J. Chan[1], Azmat Ullah[3], Jingxi Pan[4,5], Christoph H. Borchers[4,5], John E Burke[5], Christopher Stefan[6], Gertien J. Smits[3] and Christopher J.R. Loewen[1,7]

[1]Department of Cellular and Physiological Sciences, Life Sciences Institute, University of British Columbia, 2350 Health Sciences Mall, Vancouver, British Columbia, V6T 1Z3, Canada.

[2]MRC Laboratory for Molecular Biology, Francis Crick Avenue, Cambridge, CB2 0QH, United Kingdom.

[3]Department of Molecular Biology and Microbial Food Safety, Swammerdam Institute for Life Sciences, University of Amsterdam, Amsterdam, 1018 WV, The Netherlands.

[4]University of Victoria-Genome British Columbia Proteomics Centre, Vancouver Island Technology Park, #3101-4464 Markham St., Victoria, BC V8Z 7X8, Canada

[5]Department of Biochemistry & Microbiology, University of Victoria, 3800 Finnerty Rd., Victoria, BC V8P 5C2, Canada

[6]MRC Laboratory for Molecular Cell Biology, University College London, Gower Street, London, WC1E 6BT, United Kingdom.

[7]Correspondence should be addressed to C.J.R.L. (email: christopher.loewen@ubc.ca)

Lead Contact: Christopher Loewen

Abstract

Phosphoinositides, diacylglycerolpyrophosphate, ceramide-1-phosphate and phosphatidic acid belong to a unique class of membrane signaling lipids that contain phosphomonoesters in their headgroups having pK_a values in the physiological range. The phosphomonoester headgroup of phosphatidic acid enables this lipid to act as a pH biosensor as changes in its protonation state with intracellular pH regulate binding to effector proteins. Here, we demonstrate that binding of pleckstrin homology (PH) domains to phosphatidylinositol 4-phosphate (PI4P) in the yeast *trans*-Golgi network (TGN) is dependent on intracellular pH, indicating PI4P is a pH biosensor. pH biosensing by TGN PI4P in response to nutrient availability governs protein sorting at the TGN, likely by regulating sterol transfer to the TGN by Osh1, a member of the conserved oxysterol-binding protein (OSBP) family of lipid transfer proteins. Thus, pH biosensing by TGN PI4P allows for direct metabolic regulation of protein trafficking and cell growth.

Introduction

Phosphoinositides play important signaling roles in cells by recruiting cytoplasmic effector proteins to distinct intracellular membranes. Effector proteins interact with phosphoinositides using a limited set of highly conserved phosphoinositide recognition domains that enable high affinity, stereospecific recognition of individual phosphoinositide forms (Ferguson et al., 1995; Lemmon, 2008). Phosphoinositide headgroup recognition involves both electrostatic and hydrogen bonding interactions between the positively charged lysine and arginine residues that line the binding pocket and the negatively charged phosphomonoesters of the inositol ring, as well as hydrogen bonding with the ring itself (Lemmon, 2008).

The nature of the interactions with the ring phosphomonoesters suggests that the electrostatic/hydrogen bond switch mechanism, which describes how proteins bind preferentially to deprotonated phosphatidic acid (PA) (Kooijman et al., 2007), is likely relevant to phosphoinositide-protein interactions. In electrostatic/hydrogen bond switching, hydrogen bonding between the basic amino acid side chains in the protein and the phosphate oxygens of the lipid headgroup stabilizes the negative charge on these oxygens, decreasing the pK_a of the remaining proton, facilitating its dissociation (Kooijman et al., 2007). Dissociation of the proton increases the net negative charge on the phosphate, increasing the strength of electrostatic interactions with the protein to enhance lipid-protein binding.

Biochemically, electrostatic/hydrogen bond switching predicts that such lipid-protein interactions should be pH-dependent if the pK_a of the phosphomonoester lipid head group lies within the physiological range. This is because the protein will have higher affinity for the deprotonated form of the phosphomonoester lipid headgroup, which predominates at pHs greater than the pK_a. Indeed, this has been demonstrated for PA and its binding to a yeast transcription factor Opi1 (Young et al., 2010). Opi1 binds to PA located in the ER when cytoplasmic pH (pH_c) is ~7, which prevents entry of Opi1 into the nucleus. When pH_c decreases in response to glucose starvation, Opi1 unbinds PA, translocates into the nucleus and represses over 30 genes involved in phospholipid synthesis, hence, coupling nutrient availability to membrane biogenesis and cell growth.

Since the pK_a values of the headgroup phosphomonoesters of phosphoinositides also reside in the physiological range (close to 7) (Kooijman et al., 2009; van Paridon et al., 1986), selective binding of phosphoinositide recognition domains to the deprotonated phosphoinositide forms

could enable regulation by intracellular pH (pH_c). To investigate roles for phosphoinositides as pH biosensors, we focused on PH domains from the oxysterol-binding protein (OSBP) family of tethering proteins and their binding to PI4P in the yeast TGN. The OSBP-related proteins (ORPs) are a highly conserved family of seven proteins in yeast (Osh1-Osh7) and sixteen in humans that function as intracellular lipid transfer proteins that transfer phospholipids and sterols between the endoplasmic reticulum and other intracellular membranes using a PI4P counter-transport mechanism at membrane contact sites, regions of close contact between the ER and other intracellular membranes (Chung et al., 2015; Mesmin et al., 2013; Moser von Filseck et al., 2015). OSBP itself transports cholesterol from its site of synthesis in the ER to the TGN at ER-TGN contacts (Mesmin et al., 2013). Localization of OSBP to ER-TGN contacts is mediated by interaction of its FFAT motif with its ER receptor VAP and by interaction of its PH domain with TGN PI4P and Arf1, while cholesterol/PI4P counter-transport by OSBP is mediated by its OR domain, a domain common to all ORPs (Mesmin et al., 2013). Osh1 is a close yeast homolog to OSBP (Raychaudhuri and Prinz, 2010) and similar to OSBP, Osh1 contains a FFAT motif and a PH domain that likely localizes it to ER-TGN contacts (Loewen et al., 2003) and an OR domain that competitively binds ergosterol and PI4P (Manik et al., 2017). We find that the interaction of the PH domains from human OSBP, Osh1, and Osh2 with TGN PI4P is sensitive to cytoplasmic acidification and that this regulates sorting of the Tat2 amino acid permease at the TGN, likely as a result of sterol transfer from the ER to TGN by Osh1.

Results

Direct binding of PH domains to PI4P is dependent on pH and the protonation state of the phosphate headgroup

We first investigated whether the direct interaction of PH^{OSBP} and PH^{Osh1} with PI4P was pH-

sensitive. We bound purified recombinant PH^{OSBP} and PH^{Osh1} to liposomes containing PI4P at varying pH values. In both cases, binding decreased as pH was lowered (Figures 1A and 1B). Binding to PI4P was specific because mutation of two consecutive basic residues in the ß1-ß2 loop that interact with the 4-phosphate of the inositol headgroup prevented binding (Levine and Munro, 2001; 2002) (Figures 1C and 1D). The pH-dependent binding suggested that the affinity of PH^{OSBP} and PH^{Osh1} for PI4P lowered as the negative charge on the lipid headgroup decreased, consistent with the electrostatic/hydrogen bond switch mechanism (Kooijman et al., 2007). This suggested that PI4P acted as a pH biosensor. It was also conceivable that the structure of the PH domain changed with a decrease in pH, which decreased the binding affinity for PI4P. However, using hydrogen deuterium exchange mass spectrometry with purified PH^{OSBP}, we did not observe any structural changes that might be indicative of pH-sensing by the protein (Figure S1).

If a change in the ionization state of PI4P was responsible for the observed pH-dependent binding to PH^{OSBP} and PH^{Osh1} then binding should depend on the pK_a of the 4-phosphate. PH^{OSBP} binds to both PI4P and phosphatidylinositol 4,5-bisphosphate (PIP_2) with equal affinity in vitro (Levine and Munro, 2002). Binding to both PI4P and PIP_2 requires the same two basic residues in PH^{OSBP}, which interact with the 4-phosphate of the headgroup (Levine and Munro, 2002), indicating that binding of PH^{OSBP} to PIP_2 is via its 4-phosphate. Ionization of the 4-phosphate of PIP_2 is more complex than PI4P, due to the sharing of the remaining proton between the two vicinal phosphomonoester groups, which stabilizes this proton (Kooijman et al., 2009) (Figure 1F). This results in the 4-phosphate of PIP_2 carrying less negative charge than PI4P over the physiological pH range (Kooijman et al., 2009) (Figure 1E). Therefore, binding of PH^{OSBP} to PIP_2 should be more sensitive to acidification over this range if binding is dependent on the charge on the 4-phosphate. First, we verified that binding of PH^{OSBP} to PIP_2 involved the

same set of interactions as PI4P. At high pH (pH 8.5), when the 4-phosphate of PI4P and PIP_2 should be fully deprotonated, binding to PIP_2 was similar to binding to PI4P and required the same basic amino acids (Figure 1C), consistent with PH^{OSBP} primarily interacting with the 4-phosphate of PIP_2. Now we examined pH-dependence of binding. Binding of PH^{OSBP} to PIP_2 was clearly more sensitive to acidification than binding to PI4P (Figure 1G). At pH 7.6 binding to PIP_2 was reduced by ~ 50% relative to pH 8 whereas binding to PI4P remained unchanged, and at pH 7.2 binding to PIP_2 was reduced by ~ 80% compared to a ~ 30% reduction for PI4P (Figure 1H). Thus, the increased sensitivity to pH of the binding of PH^{OSBP} to PIP2 supported that pH-dependent binding depended on the ionization state of the 4-phosphate, consistent with the lipid acting as the pH sensor.

PH domain binding to TGN PI4P is pH-dependent

Now we tested whether binding of the PH domains to TGN PI4P *in vivo* was pH-sensitive. We first confirmed that the PH domains from human OSBP (GFP-PH^{OSBP}) and the yeast homologue, Osh1 (GFP-PH^{Osh1}), localized to the yeast TGN. Both GFP-PH^{OSBP} and GFP-PH^{Osh1} localized to punctate structures characteristic of the yeast Golgi, which coincided with the TGN marker Sec7-RFP (Faulhammer et al., 2007) (Figure 2A). Using a temperature-sensitive mutant of the Golgi-localized PI-4 kinase, Pik1, which results in reduced levels of TGN PI4P at the non-permissive temperature (Fairn et al., 2007), we found that binding of GFP-PH^{OSBP} and GFP-PH^{Osh1} to the TGN was dependent on TGN PI4P levels (Figures S2A to S2D). Now we tested for a role for pH. The drug ebselen is an inhibitor of the plasma membrane (PM) P-type H^+ ATPase, Pma1, and ebselen addition rapidly acidifies pH_c to ~ 6 (Chan et al., 2007; Young et al., 2010). Upon ebselen addition, we observed delocalization of both GFP-PH^{OSBP} and GFP-PH^{Osh1} from the TGN to the cytoplasm (Figure 2B), suggesting binding to the TGN was pH-sensitive. Next,

we treated yeast with the protonophore 2,4-dinitrophenol (2,4-DNP) over a range of pH values and quantified TGN localization. Both GFP-PH^{OSBP} and GFP-PH^{Osh1} delocalized from the TGN as pH_c decreased, which titrated over the physiological range (Figures 2C to 2E). GFP-PH^{OSBP} appeared to be slightly more sensitive to acidification at pH 6.8 compared to GFP-PH^{Osh1}, whereas both PH domains showed the same degree of delocalization at pH 6 and 6.4. Sec7-RFP was unaffected by cytoplasmic acidification, indicating that the TGN remained intact with decreasing pH_c (Figures S2E and S2F). Arf1 and TGN PI4P coincidentally target PH^{OSBP} and GFP-PH^{Osh1} to the TGN (Godi et al., 2004; Levine and Munro, 2002; Roy and Levine, 2004). We found that the localization of Arf1-GFP was unaffected by decreased pH_c (Figures S2G and S2H), indicating that Arf1 likely did not play a role in pH-dependent binding of proteins to TGN PI4P. We were unable to detect direct binding between yeast Arf1 and PH^{Osh1} (Figure S3) suggesting the previously found role for Arf1 in targeting PH^{Osh1} to the TGN (Levine and Munro, 2002; Roy and Levine, 2004) may be indirect, perhaps because Arf mutants have reduced PI4P (Audhya et al., 2000). The lack of direct binding between Arf1 and PH^{Osh1} provided additional evidence that Arf1 did not play a role in pH-dependent binding of PH^{Osh1} to the TGN. Additionally, we tested another PI4P probe, GFP-$PH^{Osh2\text{-}dimer}$, which is a tandem dimer of the Osh2 PH domain that binds both TGN and PM pools of PI4P, but does not bind Arf1 (Roy and Levine, 2004). This probe was sensitive to cytoplasmic acidification upon ebselen treatment and delocalized from both the TGN and PM (Figure 2F), further supporting that Arf1 was not required.

To examine the physiological effects of pH on TGN PI4P, we used a genetically encoded pH-sensitive mutant, *pma1-007*, which has 50% reduced expression and activity of the Pma1 proton pump and renders yeast susceptible to cytoplasmic acidification when grown under conditions of acid stress (Orij et al., 2012; Peters et al., 2013; Young et al., 2010). When grown

on pH 5 media *pma1-007* pH_c is neutral (~7), but when grown on pH 4 or 3 media pH_c becomes acidified (~6.9 and 6.8 respectively; compared to ~7.1 for wild type) (Young et al., 2010). Under non-acid-stressing conditions in the *pma1-007* mutant (pH 5 medium), localization of GFP-PH^{Osh1} to the TGN was no different than wild type (Figures 2G and 2H). However, under acid stress (pH 3 medium), localization to the TGN was dramatically reduced in the *pma1-007* mutant. Localization of GFP-$PH^{Osh2\text{-}dimer}$ to the TGN was also dramatically reduced under acid stress (Figures 2I and 2J).

We now sought to rule out the possibility that TGN PI4P decreased upon cytoplasmic acidification. We measured total cellular PI4P levels by HPLC and found no significant decrease between cells treated with 2,4-DNP at pH 6 and pH 7.2, in which pH_c is the same as the buffer pH (Figure 2K). We also measured PI4P levels in the *pma1-007* mutant under acid stress (pH 4 media) and found no decrease in PI4P compared to wild type (Figure 2L; we chose pH 4 media because yeast growth assays had to be performed at this pH – see Figure 7 – and because at this media pH, pH_c is lowered from ~7.1 to ~6.9 (Young et al., 2010)). Finally, using a *sac1^{ts} Δsjl2 Δsjl3* phosphoinositide polyphosphatase triple mutant, which blocks PI4P turnover and has a ~ 25 fold elevation of PI4P (Foti et al., 2001), we found no difference in release of GFP-PH^{OSBP} from the TGN upon acidification by ebselen or 2,4-DNP (Figures S2I to S2L). Thus, cytoplasmic acidification prevented PH domain binding to TGN PI4P without causing a decrease in the level of PI4P, supporting that increased protonation of TGN PI4P under acid stress was the cause.

Glucose provides a signal for pH biosensing by PI4P

We now investigated a physiological context for pH biosensing by PI4P. Glucose is a potent regulator of pH_c, whereby glucose starvation inactivates Pma1 causing a rapid drop in pH_c to ~ 6 (Martínez-Muñoz and Kane, 2008; Young et al., 2010). Thus, glucose might regulate binding of PH domains to the TGN. We quantified the localization of PH^{Osh1} and PH^{OSBP} to the TGN upon glucose starvation and found that both delocalized in wild type cells over a similar timescale as the drop in pH_c (Figures 3A and 3B; and S3A and S3B; compare to Figure 4E for change in pH_c) (Young et al., 2010). In fact, translocation was largely complete by 15min at which point pH_c was ~ 6.2 (Figure 4E) corresponding to a > 50% decrease in deprotonated PI4P (Figure 1E). This is consistent with glucose acting via a change in pH_c. The function of PI4P in the TGN is thought to be regulated primarily through its synthesis and degradation. The TGN-localized Pik1 kinase is responsible for synthesis of this pool of PI4P, which accounts for ~ 50% of total cellular PI4P and is distinct from the PM pool generated by the PM-localized Stt4 PI-4 kinase (Audhya et al., 2000). Glucose regulates localization of Pik1 to the TGN, such that glucose starvation causes dissociation of Pik1 from the TGN, implying that the level of TGN PI4P decreases upon glucose starvation (Demmel et al., 2008; Faulhammer et al., 2007). The ER-localized phosphatase Sac1, which in nutrient replete conditions resides in the ER (Foti et al., 2001; Stefan et al., 2011), traffics to the TGN upon glucose starvation on a similar timescale as Pik1 dissociation and is thought to also contribute to decreased TGN PI4P (Faulhammer et al., 2007; 2005). However, because it has not been possible to measure PI4P isolated directly from the TGN, changes in PI4P in these studies were monitored indirectly using the FAPP1 PH domain (Faulhammer et al., 2005; 2007), which may also be sensitive to cytoplasmic acidification.

We sought to determine if the change in pH_c was sufficient to transmit the glucose starvation signal. First, we monitored translocation of PH^{OSBP} and PH^{Osh1} from the TGN in Δ*sac1* cells and

found no significant inhibition of the translocation of these PH domains in response to glucose starvation (Figures 3A and 3B; and S3A and S3B). This suggested that other PI phosphatases might act to reduce TGN PI4P upon glucose starvation. Hence, we monitored translocation of PH^{OSBP} in the *sac1^{ts} Δsjl2 Δsjl3* triple mutant, which completely blocks PI4P turnover. We found no difference in PH^{OSBP} translocation compared to controls, thereby ruling out a role for the PI phosphatases in PI4P elimination in the TGN (Figures 3C and 3D).

Now we tested a role for Pik1 in PH domain translocation (Figures 3F and 3G). The compound phenylarsine oxide (PAO) is a PI-4 kinase Type III inhibitor (Barylko et al., 2001; Wiedemann et al., 1996) and we determined whether we could use it to acutely inhibit PI4P synthesis in the yeast TGN. PAO treatment for 15 and 30 min in the presence of glucose resulted in a time-dependent decrease in TGN PI4P, as measured using the GFP-$PH^{Osh2\text{-}dimer}$ probe (compare i, ii and iii). Localization of GFP-$PH^{Osh2\text{-}dimer}$ to the PM was not reduced by PAO (iii), indicating PAO specifically inhibited Pik1. Now we measured the effects of PAO addition during glucose starvation. Similar to PH^{OSBP} and PH^{OSH1}, we found that GFP-$PH^{Osh2\text{-}dimer}$ delocalized from the TGN after 30 min of glucose starvation (compare i and iv). We found that PAO addition after 15 min of glucose starvation (when PH domain delocalization was largely complete; Figure 3B) enhanced delocalization of GFP-$PH^{Osh2\text{-}dimer}$ from the TGN compared to glucose starvation alone (compare iv and v). This indicated that Pik1 remained active during the time-course of glucose starvation, suggesting its inactivation was not required for PH domain translocation.

If a loss in Pik1 activity and a decrease in PI4P were required to delocalize the PH domains from the TGN, then PAO treatment should prevent their relocalization upon glucose re-addition, as this would block re-synthesis of PI4P. First, we tested for relocalization of the probe upon

glucose re-addition. Adding back glucose for 5 min after 25 min of glucose starvation, which is known to restore pH_c (Martínez-Muñoz and Kane, 2008), was sufficient to completely re-establish localization of GFP-$PH^{Osh2\text{-}dimer}$ to the TGN (compare i and vi). Treatment with ebselen to inhibit Pma1 prevented relocalization upon glucose re-addition, indicating that relocalization depended on an increase in pH_c (Figures S3E and S3F). This was also true for PH^{OSBP} and PH^{Osh1} (Figures 4A and 4B and S4A and S4B). To measure relocalization to the TGN upon glucose re-addition in the presence of PAO we could not use a 30 min PAO treatment because very little probe remained localized (iii); hence we used a 15 min PAO treatment for which we observed a ~30% decrease in probe localization (ii), indicating Pik1 was effectively inhibited by this treatment. Incubation with PAO for 15 min during glucose starvation did not block relocalization to the TGN upon glucose re-addition (compare v and vii). In fact, the degree of relocalization was identical to PAO treatment in the presence of glucose (compare ii and vii). Even if Pik1 inhibition by PAO was partial over this time-course, we would have expected to see diminished relocalization compared to PAO treatment in the presence of glucose, if glucose starvation caused a substantial decrease in PI4P; this was clearly not the case. Extending PAO treatment to 30 min by imaging for a further 15 min reduced relocalization to the same level as PAO treatment for 30 min in the presence of glucose (compare iii and viii), supporting that Pik1 was inhibited by PAO similarly during the time-course of glucose starvation and re-addition. Thus, together these data supported that enough PI4P remained in the TGN during glucose starvation to allow for pH-biosensing by PI4P to occur.

We now sought a TGN marker whose localization was dependent on PI4P but was insensitive to pH_c to further support that TGN PI4P remained during glucose starvation. The Arf GEF, Sec7, physically interacts with Pik1 at the TGN (Gloor et al., 2010) and because we found its localization to be insensitive to pH_c (Figures S2E and S2F), we tested whether its localization

was also dependent on PI4P. We treated Sec7-GFP cells with PAO for 30 min and found its TGN localization was indeed sensitive to PAO (Figures 3G and 3H). Thus, Sec7 TGN localization was dependent on the level of PI4P, but insensitive to its protonation state. Now we examined Sec7 TGN localization in response to glucose starvation and found Sec7-RFP remained at the TGN even after 60 min, when PH^{OSBP} had clearly translocated (Figures 3I and 3J). If PI4P continued to be synthesized by Pik1 during glucose starvation then Sec7 localization should remain sensitive to PAO. We glucose starved cells expressing Sec7-RFP for 30 min and treated these starved cells with PAO for an additional 30min. We found that Sec7 TGN localization remained sensitive to PAO after this treatment (Figure S3G). Thus, together these data strongly supported that PI4P remained in the TGN during glucose starvation because Pik1 remained active, and that pH biosensing by PI4P regulated PH domain binding to the TGN in response to glucose.

Now we sought to modulate the pH_c change in response to glucose starvation and determine the effect on PH domain translocation. We previously found that Reg1, the glucose-signaling-specific regulatory subunit for Glc7, yeast's protein phosphatase type 1, is required to transmit the glucose starvation signal to pH_c, such that deletion of *REG1* limits the drop in pH_c by preventing Pma1 from switching-off in the absence of glucose (Young et al., 2010). This effect may be through cellular ATP levels since the drop in ATP in response to glucose starvation is attenuated in Δ*reg1* cells (Aoh et al., 2013). We measured translocation of PH^{OSBP} and PH^{OSH1} in Δ*reg1* cells and found their translocation was blocked, but remained sensitive to pH_c as ebselen addition prevented their TGN localization (Figures 4A and 4B and S4A and S4B). Because Arf1 is also known to dissociate from the TGN during glucose starvation (Aoh et al., 2013), we tested whether it was affected in Δ*reg1* cells. As expected, glucose removal caused Arf1-GFP translocation from the TGN; however, translocation was not blocked in the Δ*reg1*

mutant (Figures 4C and 4D). This indicated that PH domain translocation in response to glucose starvation was independent of Arf1, and that Arf1 dissociation was governed by a signal independent of pH_c.

Protein kinase A (PKA) is also known to play a role in pH-mediated signaling in response to glucose (Dechant et al., 2010) and in localization of clathrin adapter proteins to the TGN in response to glucose (Aoh et al., 2011). Hence, we hypothesized that PKA might play a role in regulating the change in pH_c upon glucose starvation. We investigated this using a strain called *Tpk1-as*, which is missing all catalytic subunits of PKA except for a single PKA allele that is sensitive to the inhibitor 1NM-PP1 (Aoh et al., 2013). We measured pH_c upon glucose starvation in *Tpk1-as* cells without 1NM-PP1 treatment and found, as previously, that pH_c dropped within minutes of glucose starvation, reaching pH ~ 5.7 within 60 min (Figure 4E) (Young et al., 2010). Treatment of *Tpk1-as* cells with 1NM-PP1 prior to glucose starvation resulted in a marked reduction in intracellular acidification upon glucose starvation (Figure 4E), supporting that PKA functioned in transmitting the signal from glucose to pH_c. Furthermore, treatment of *Tpk1-as* cells with 1NM-PP1 did not block cytoplasmic acidification (Figure 4F) or translocation of PH^{OSBP} in response to ebselen (Figure S4C), indicating Pma1 failed to properly switch-off during glucose starvation of 1NM-PP1-treated *Tpk1-as* cells. We now used PKA inhibition to investigate pH_c dependency in translocation of the PH domains. We found that pretreatment of *Tpk1-as* cells with 1NM-PP1 prior to glucose starvation partially prevented translocation of both PH^{OSBP} and PH^{Osh1} (Figures 4G and 4H and S4D and S4E). It was not until pH_c dropped to near or below the pK_a of PI4P (~ 6.3; (van Paridon et al., 1986)) at ~ 60 min that the PH domains significantly translocated (compare Figure 4E with Figures 4H and S4E). Thus, these data further supported that translocation of PH^{OSBP} and PH^{Osh1} from the TGN in response to glucose starvation was mediated by the decrease in pH_c.

Osh1 TGN localization is regulated by pH_c and PI4P

Now we investigated a role for pH biosensing by PI4P in regulation of Osh1 localization. Osh1 has dual localizations, to both the TGN (Daboussi et al., 2012) and the nucleus vacuole junction (NVJ) (Kvam and Goldfarb, 2004). To test the role for the PH domain in localizing Osh1 to the TGN, we mutated two consecutive arginine residues to alanine within the PH domain of full length Osh1, which prevented binding of the PH domain to PI4P *in vitro* (Figure 1D). The GFP-Osh1^{AA} mutant showed greatly reduced localization to the TGN (Figures 5A and 5B), but localization to the NVJ was unchanged (Figures 5A and 5C). Now we used the temperature-sensitive allele of the Pik1 kinase, *pik1-104*, to examine the role of TGN PI4P in Osh1 localization to the TGN. We found that the *pik1-104* mutant grown at a semi-permissive temperature of 30˚C showed specific depletion of the TGN pool of PI4P, but not PM PI4P, as measured using the GFP-PH$^{Osh2\text{-}dimer}$ probe (Figures S5A to S5C). Growing the *pik1-104* mutant at 30˚C resulted in decreased localization of GFP-Osh1 to the TGN (Figures 5D and 5E), supporting that PI4P localized GFP-Osh1 to the TGN. GFP-Osh1 localization to the NVJ was unaffected (Figure 5F).

Now we determined whether glucose and pH_c controlled binding of Osh1 to TGN PI4P. Treatment with both ebselen (Figures 5G and 5H) and 2,4-DNP (Figures 5I and 5J) resulted in dissociation of GFP-Osh1 from the TGN. GFP-Osh1 localization to the TGN in the *pma1-007* mutant was significantly decreased under acid stress (pH 3 medium), but was unaffected under non-acid-stressing conditions (pH 5 medium) (Figures 5K and 5L). Cytoplasmic acidification in *pma1-007* cells can be alleviated by deleting *REG1*, which increases Pma1 activity and raises

pH_c (Young et al., 2010). Localization of GFP-Osh1 was restored in the Δ*reg1 pma1-007* double mutant under acid stress (Figures 5K and 5L), confirming that pH_c regulated Osh1 binding to TGN PI4P. Now we examined the effect of glucose starvation on the localization of Osh1. GFP-Osh1 translocated from the TGN upon glucose starvation with similar kinetics as the PH domain alone, which was not altered by deletion of *SAC1* (Figures 5M and 5N). Localization of GFP-Osh1 to the NVJ remained unchanged after glucose starvation (Figure 5M). We also tested a role for Arf1 given its putative role in localizing PH^{Osh1} to the TGN and found that GFP-Osh1 translocated in Δ*arf1* cells in response to glucose starvation, indicating Arf was not required to transmit the pH_c signal to Osh1 (Figure S5G and S5H).

Osh1 regulates Tat2 trafficking at the TGN

Loss of Osh1 results in defective tryptophan (Trp) import and failure to grow on media with limiting Trp, although the role for Osh1 is unknown (Figure 6A) (Jiang et al., 1994). Under conditions of limiting Trp, Trp import is primarily mediated by the high affinity Trp permease, Tat2 (Schmidt et al., 1994). When Trp is abundant, Tat2 is ubiquitylated and trafficked to the vacuole for degradation (Umebayashi and Nakano, 2003). Sterol is required for proper trafficking of Tat2 to the PM, where it resides in sterol-rich membrane domains (Umebayashi and Nakano, 2003). When sterol is depleted Tat2 is ubiquitylated and re-routed from the TGN to the vacuole via the late endosome, independent of the PM (Umebayashi and Nakano, 2003). Hence, Osh1 function in sterol traffic at the TGN might be important for Tat2 sorting at the TGN. We examined whether Trp import was dependent on Osh1 binding to TGN PI4P. GFP-$Osh1^{AA}$ failed to rescue the Trp sensitivity of Δ*osh1* cells (Figure 6B), supporting that binding of Osh1 to TGN PI4P regulated Trp import. Now we used the temperature-sensitive allele of the Pik1 kinase, *pik1-104*, to examine the role of TGN PI4P in Trp import. We found that the *pik1-104*

mutant grown at the semi-permissive temperature of 30˚C, which we demonstrated had specific depletion of the TGN PI4P, resulted in poor growth on media with low Trp (Figure 6C). PI4P levels measured by HPLC and using the GFP-PH$^{Osh2\text{-}dimer}$ probe were unchanged in Δ*osh1* cells indicating Osh1 was not required for Pik1 activity (Figures 2L and S5D to S5F). PM-localized Tat2-GFP was greatly reduced in Δ*osh1* cells (Figures 6D and 6E). Correspondingly, over-expression of Tat2-GFP from a plasmid rescued the Trp sensitivity of the Δ*osh1* mutant (Figure 6F), confirming that Trp sensitivity resulted from decreased Tat2 at the PM in the absence of Osh1. Thus, binding of Osh1 to TGN PI4P was required for Trp uptake by promoting trafficking of Tat2 to the PM.

The role for Osh1 in Tat2 trafficking suggested Osh1 might be generally required for trafficking at the TGN and if so should show genetic interactions with trafficking genes. We queried the global genetic interaction map, a matrix of nearly one million pairwise genetic interactions covering all yeast bioprocesses, for *OSH1* interactions (Costanzo et al., 2016). *OSH1* has 105 aggravating and 88 alleviating genetic interactions (Table S1), and we searched for functional enrichment within these interactions (Figure 6G and Table S2). We found that both aggravating and alleviating interactions for *OSH1* were enriched for trafficking-related components, with functions related to Golgi, TGN, endosomal transport, membrane fusion, sporulation, and autophagy. Thus, the genetic interaction profile for *OSH1* provided additional unbiased evidence for a role for Osh1 in trafficking at the TGN.

Glucose and pH_c regulates Tat2 trafficking and Trp uptake via TGN-localized Osh1

Now we investigated a role for pH_c in regulation of Osh1 and Tat2 trafficking. We found that the

pma1-007 mutant grew poorly in low Trp media at low pH (pH 4), which was rescued by deletion of *REG1* (Figure 7A), supporting that decreased pH_c impaired Trp import. Growth of *pma1-007* on pH 5 medium also rescued Trp sensitivity (Figure 7B). We confirmed decreased PM levels of the Tat2 permease under acid stress (Figures 7C and 7D), consistent with the Trp phenotype, and that overexpression of Tat2-GFP rescued deficient Trp uptake (Figure 7E). If decreased Tat2 trafficking in response to cytoplasmic acidification resulted from decreased binding of Osh1 to TGN PI4P, then increasing the levels of Osh1 should rescue the Trp sensitivity phenotype through binding to the remaining deprotonated TGN PI4P. We tested this by overexpressing GFP-Osh1 in *pma1-007* cells and found that Osh1 overexpression rescued its Trp sensitivity (Figure 7F). Overexpression of the PI4P binding-defective GFP-Osh1^{AA} mutant failed to rescue (Figure 7F), indicating that decreased binding of Osh1 to TGN PI4P under acid stress caused defective Trp import. Thus, pH_c controlled Osh1 binding to TGN PI4P, which regulated Tat2 trafficking and amino acid import.

Now we tested for a role for glucose in Tat2 trafficking. Glucose starvation has been previously shown to lead to Tat2 degradation in the vacuole via a route independent of the PM, suggesting Tat2 takes a direct route from TGN to the vacuole (Beck et al., 1999). We found that glucose starvation resulted in a decrease in PM-localized Tat2-GFP that occurred within minutes of glucose removal, which was partially restored within 10 minutes of re-addition of glucose (Figure 7G and H). Ebselen addition blocked Tat2-GFP PM relocalization, indicating an increase in pH_c upon glucose re-addition was required. We noticed that within 15min of glucose starvation Tat2-GFP also localized to punctate structures that appeared to be adjacent to vacuoles, suggesting these were late endosomes. Thus, we colocalized Tat2-GFP with the marker Snf7-RFP and found indeed that these were late endosomes (Fig 7I). We also colocalized with Sec7-RFP and found none of the puncta coincided with TGN (Fig 7J) indicating that glucose starvation did not

block trafficking of Tat2-GFP out of the TGN. Taken together, these results supported that glucose regulated sorting of Tat2 at the TGN towards the PM in presence of glucose or towards late endosomes in its absence, which was dependent on pH_c.

If pH_c regulated the function of TGN PI4P, then cytoplasmic acidification should aggravate growth of the *pik1-104* mutant, given that Pik1 plays an essential role at the TGN (Fairn et al., 2007). We generated a *pik1-104 pma1-007* double mutant strain to introduce acid stress into *pik1-104* cells, and consistent with pH_c regulating the function of TGN PI4P, *pik1-104 pma1-007* double mutant cells incubated at the semi-permissive temperature grew worse than either of the single mutants under acid stress (Figure 7K). Thus, pH_c regulated the activity of PI4P in the TGN.

Discussion

The phosphoinositide class of signaling lipids contain phosphomonoesters in their headgroup that are critical for their stereo-specific interaction with effector proteins. These headgroup phosphomonoesters have pK_a values in the physiological range, implying they may sense changes in pH (Kooijman et al., 2009; van Paridon et al., 1986). We show that changes in pH regulate the direct binding of effector proteins of the PH domain class to PI4P both *in vitro* and *in vivo*. This binding is dependent on the ionization state of the phosphomonoester headgroup, not a conformational change in the protein, making PI4P a lipid pH biosensor. pH biosensing is possible because of electrostatic/hydrogen bond switching between the basic side chains of the protein and the phosphomonoesters of the lipid (Kooijman et al., 2007), whereby increased

charge on the phosphomonoester strengthens both the electrostatic and hydrogen bonding interactions with the protein, increasing the overall affinity for the lipid. Hence, a decrease in pH_c leads to decreased charge on the lipid headgroup and reduced effector protein binding, enabling the lipid-protein interaction to be a molecular pH sensor.

We find that glucose availability is a physiological signal for pH biosensing by PI4P, which regulates Osh1 binding to TGN PI4P over a timescale of minutes. This allows pH biosensing by TGN PI4P to be instantaneous and reversible. pH biosensing by TGN PI4P in response to glucose regulates trafficking of the high affinity tryptophan permease Tat2 to the PM, which serves to restrict amino acid uptake and cell growth under nutrient limiting conditions. Hence, pH biosensing by PI4P, similar to pH biosensing by PA (Young et al., 2010), is an important signaling mechanism coupling the metabolic status of the cell (via pH) to nutrient uptake and cell growth. pH biosensing by PI4P is clearly a distinct mechanism from pH biosensing by PA given that PI4P uses a distinct effector protein, Osh1, which is not known to bind PA and lacks PA-binding domains. pH biosensing by PI4P/Osh1 also has a distinct location at the TGN, whereas pH biosensing by PA/Opi1 occurs at the ER where there is little/no PI4P. However, because both pathways utilize pH biosensing in response to glucose availability, this suggests they cooperate to restrict cell growth by coordinately regulating lipid synthesis (for PA/Opi1) and protein sorting/trafficking at the TGN. pH_c has been found to regulate trafficking at the TGN in cultured fibroblasts, although the mechanism is unknown (Cosson et al., 1989) and our work suggests that pH biosensing by PI4P in the mammalian TGN may also play a role, given the highly conserved function for this lipid and the similar function of OSBP at the TGN (Mesmin et al., 2013).

Pik1 delocalizes from the TGN upon glucose removal over a similar timescale as pH biosensing (Aoh et al., 2013). Although Pik1 delocalization and lowering of TGN PI4P may synergize with pH biosensing by PI4P, we show that pH biosensing by PI4P is sufficient to transduce the pH signal to Osh1. This suggests that Pik1 delocalization may also serve an additional function during glucose starvation. Pik1 TGN localization is dependent on binding to the adapter Gga2 (Daboussi et al., 2017), which drives synthesis of PI4P and adapter progression in the TGN (Daboussi et al., 2012; 2017). Gga2 along with the adapters Apl4, Ent3, and Ent5, delocalize on a similar timescale during glucose starvation (Aoh et al., 2011; 2013). However, after prolonged glucose starvation of 2-3 hours, adapters and clathrin relocalize to the TGN, but Pik1 does not (Aoh et al., 2011; 2013) (neither do the PH domains – unpublished data). Thus, it is likely that delocalization of Gga2, Apl4, Ent3, and Ent5 adapters together with Pik1 halts secretion, and the persistent delocalization of Pik1 maintains a block on secretion even after adapters have relocalized. Adapter relocalization prior to glucose re-addition would prime the TGN, awaiting relocalization of Pik1 and resumption of PI4P production in the TGN upon glucose re-addition. Arf1 recruitment to the TGN is an early event in adapter progression (Daboussi et al., 2012). Arf1 also delocalizes upon glucose starvation over the same timescale as adapters and Pik1, but does not relocalize after prolonged glucose starvation (Aoh et al., 2013), suggesting the absence of Arf1 may also play a role in maintaining the block on secretion. Because we find Arf1 TGN localization to be pH_c-insensitive and uncoupled from the glucose starvation pH signal, a separate pH_c-insulated factor likely regulates Arf1 localization in response to glucose. Sec7 is a strong candidate because it directly recruits Arf1 to the TGN (Richardson et al., 2016) and we find that Sec7 localization is insensitive to both cytoplasmic acidification and glucose starvation. Sec7 also interacts with Pik1 (Gloor et al., 2010) and could regulate its TGN localization in response to glucose.

Sterol transfer by OSBP is driven by coupled counter-transport of PI4P and PI4P hydrolysis by Sac1 in the ER (Mesmin et al., 2013). Sterol transfer also requires interaction with VAP proteins in the ER, via the FFAT motif in OSBP (Mesmin et al., 2013). Given that Osh1 competitively binds sterols and PI4P in its OR domain (Manik et al., 2017), we propose it acts to transfer sterols from the ER to TGN similarly to OSBP (Figure 7J). Decreased sterol transfer to the TGN in the Δ*osh1* mutant and in cells experiencing acid stress, in which Osh1 is delocalized, would explain the defects in Tat2 trafficking, given that Tat2 trafficking to the PM relies on TGN sterols (Umebayashi and Nakano, 2003). We rule out a role for sterol transfer at the NVJ in Tat2 trafficking since Osh1 localization to the NVJ is unaffected in the TGN-delocalized Osh1^{AA} mutant. Additionally, loss of Nvj1, the NVJ binding partner for Osh1, does not result in defective Trp uptake (Kvam and Goldfarb, 2006). Binding to the VAP ortholog Scs2 is required for Trp uptake (mutation of the FFAT motif in Osh1 causes Trp sensitivity (Loewen et al., 2003)), further supporting that sterol transfer originates in the ER. ER-TGN contacts have now been defined ultrastructurally in yeast through characterization of the integral ER tethering protein, Nvj2, which transfers ceramide from ER to Golgi (Liu et al., 2017). Hence, it is possible that Osh1 acts by bridging ER-TGN contacts through simultaneous binding of Scs2 in the ER and PI4P in the TGN, similarly to OSBP, facilitating sterol transfer to the TGN and cargo sorting. We propose that pH_c is also a regulator of recruitment of proteins to membrane contact sites.

If indeed Osh1 transfers sterol to the TGN, then loss of Osh1 should produce sterol trafficking defects. Fenpropimorph is an antifungal that is an inhibitor of sterol biosynthesis, and yeast with defects in sterol synthesis are fenpropimorph-sensitive (Marcireau et al., 1990). Fenpropimorph resistance, however, arises from defects in trafficking of sterols and sphingolipids to the PM (Stolz and Sauer, 1999). Δ*osh1* cells have normal levels of ergosterol and the biosynthetic precursors lanosterol and zymosterol (Beh et al., 2001); however, consistent with a role for

Osh1 in sterol trafficking, Δ*osh1* cells are fenpropimorph resistant (Toulmay and Prinz, 2012). Sterols are required for trafficking at the TGN and many Golgi trafficking components show aggravating genetic interactions with sterol synthesis genes. Examining genetic interactions for *OSH1* (Table S1 and Figure 6G), the strongest aggravating interaction with *OSH1* is with *GOS1* (SGA Score -0.511), a v-SNARE required for Golgi transport. *OSH1* also shows strong aggravating interactions with other trafficking components, including *AGE2* (Arf GAP effector), *VPS41* (HOPS endocytic tethering complex), *Sla2* (clathrin adapter protein) and *COG4* (COG Golgi vesicle tethering complex). Many of these genes also show aggravating genetic interactions with sterol synthesis genes (for example, *AGE2* interacts strongly with *ERG24* (SGA Score -0.682) and *ERG3*, and moderately with *ERG2*, *ERG11*, *ERG13* and *ERG26* (http://thecellmap.org) (Costanzo et al., 2016). Thus, the genetic interactions between *OSH1* and the same trafficking components that interact with sterol synthesis genes further support a role for Osh1 in ER to TGN sterol transport.

Cytoplasmic pH is emerging as an important signal regulating cell growth in yeast and humans (Dechant et al., 2010; 2014; Isom et al., 2013; Orij et al., 2012), and is especially important in cancer cell metabolism where it is a therapeutic target (Cardone et al., 2005; Sin et al., 2009). Thus, pH biosensing by PI4P in combination with different effector proteins likely represents an important mechanism for transmitting changes in cytoplasmic pH to a diverse network of cellular effectors. That other phosphoinositides have pK_as in the physiological range implies that pH biosensing by PIPs is not limited to PI4P and will likely impact aspects of phosphoinositide signaling in many pathways in many organisms.

Acknowledgements

We thank P. Mayinger for the Sec7-RFP plasmid, A. Nakano for the Tat2-GFP plasmid, and M.C. Duncan for the *tpk1-as* mutant. This research was supported by grants from the National Sciences and Engineering Council of Canada (NSERC), the Canadian Institute of Health Research (CIHR), the Michael Smith Foundation for Health Research (MSFHR), the Canada Foundation for Innovation, and the British Columbia Knowledge Development Fund. J.J.H.S. is the recipient of a NSERC Alexander Graham Bell Canada Graduate Scholarship and European Molecular Biology Organization long-term fellowship.

Author Contributions

Conceptualization, J.J.H.S., P.L. and C.J.R.L.; Methodology, J.J.H.S., P.L., C.S., J.E.B., C.H.B., G.S. and C.J.R.L.; Formal Analysis, J.J.H.S., P.L. and C.J.R.L.; Investigation, J.J.H.S., P.L., L.J.C., A.U., J.P., C.S. and C.J.R.L.; Writing – Orignal Draft, J.J.H.S., and C.J.R.L.; Writing – Reviewing and Editing, J.J.H.S., and C.J.R.L.; Supervision, C.J.R.L; Funding Acquisition, C.J.R.L.; Resources, C.J.R.L.;

Declaration of Interests

The authors declare no competing interests.

Main Figure Legends

Figure 1. PH domain binding to PI4P is dependent on its protonation state. (A,B) Coomassie-stained gels showing the binding of PH^{OSBP} (A) and PH^{Osh1} (B) to liposomes containing 3.5 mol% and 3 mol% PI4P at the indicated pH. 100% input represents the total amount of protein used in each binding reaction. (C) Binding of PH^{OSBP} (WT) and $PH^{OSBP(R107A, R108A)}$ (AA) to liposomes containing either 3.0 mol% PI4P or 3.0 mol% PIP_2 at pH 8.5. (D) Binding of PH^{Osh1} (WT) and $PH^{Osh1(K289A, K290A)}$ (AA) to liposomes containing 3.0 mol% PI4P at pH 7.6. WT, wild type. (E) Degree of deprotonation of the 4-phosphate of PI4P and PIP_2 versus pH. Values for PI4P are calculated based on a pK_a of 6.3 for PI4P (van Paridon et al., 1986). Measured values for PIP_2 were taken from (Kooijman et al., 2009). (F) Schematics of the major ionization species of PI4P and PIP_2 at pH 7. Dashed red lines indicate hydrogen bonds, dashed blue lines indicate covalent interactions shared between the vicinal phosphate oxygens. (G) Coomassie-stained gels showing the binding of PH^{OSBP} to liposomes containing either 1.5 mol% PI4P or 1.5 mol % PIP_2 over a range of pH. (H) Quantification of binding experiments performed in (G) (*, versus PI4P at given pH, $P < 0.05$; error bars indicate SD). See also Figure S1.

Figure 2. PH domain binding to TGN PI4P is dependent on pH_c. (A) Confocal micrographs of yeast showing the co-localization of GFP-PH^{OSBP} and GFP-PH^{Osh1} with the TGN marker Sec7-RFP. (B) Delocalization of GFP-PH^{OSBP} and GFP-PH^{Osh1} from the TGN 5 min after addition of 100 µM ebselen. (C) Delocalization of GFP-PH^{OSBP} and GFP-PH^{Osh1} 10 min after incubation with 2 mM 2,4-DNP buffered at pH 6, but not pH 7.2. (D,E) Quantification of TGN localization for GFP-PH^{OSBP} (D) and GFP-PH^{Osh1} (E) incubated with 2,4-DNP buffered over a range in pH (*, versus the higher pH, $P < 0.0005$). (F) Delocalization of GFP-$PH^{Osh2\text{-}dimer}$ from the TGN 5 min after addition of 100 µM ebselen. (G) Localization of GFP-PH^{Osh1} in WT versus *pma1-007* mutant grown in pH 5 versus pH 3 buffered medium. (H) Quantification of GFP-PH^{Osh1} TGN localization in (G) (*, versus pH 5, $P < 0.0001$). (I) Localization of GFP-$PH^{Osh2\text{-}dimer}$ in WT versus

pma1-007 mutants grown in pH 5 versus pH 3 buffered medium. (J) Quantification of GFP-PH$^{Osh2\text{-}dimer}$ TGN localization in (I) (*, versus pH 5, P < 0.0001). (K) Phosphoinositide levels measured by HPLC in cells treated with 2,4-DNP buffered at pH 7.2 and 6. (L) Phosphoinositide levels measured in WT, Δ*osh1* and *pma1-007* mutants grown in pH 4-buffered medium (*, versus WT, P < 0.05). Scale bars, 4 μm. WT, wild type. Cyto, cytoplasmic. All error bars, SEM; except in (K,L), SD. See also Figure S2.

Figure 3. Glucose regulates binding of PH domains to the TGN independent of Sac1 and Pik1. (A) Confocal micrographs of WT and Δ*sac1* cells expressing GFP-PH^{Osh1} and incubation in medium lacking glucose for the indicated times. (B) Quantification of GFP-PH^{Osh1} TGN localization in (A) (*, versus WT at given time, P < 0.05). (C,D) Same as in (A,B) except for WT and *sac1^{ts} Δsjl2 Δsjl3* triple mutant cells expressing GFP-PH^{OSBP}. (E) Pik1 inhibition assay. Confocal micrographs of WT yeast expressing GFP-PH$^{Osh2\text{-}dimer}$ grown in the presence or absence of glucose and treated with PAO. For +Glucose treatments, cells were incubated with PAO for the indicated times (i, ii, iii). For -Glucose treatments, cells were incubated without glucose for 15min prior to addition of PAO (or no addition) for 15min (iv, v). For glucose re-addition (reGlucose) without PAO treatment (vi), glucose was added for 5min after 25 min of glucose starvation. For PAO treatment (vii), PAO was added after 15min of glucose starvation prior to glucose re-addition. These cells were also imaged for an additional 15min (viii). (F) Quantification of TGN localization of GFP-PH$^{Osh2\text{-}dimer}$ in (E). Roman numerals correspond to the treatments in E. Grey lines connecting treatments indicate lack of significance, P > 0.1; all other treatment comparisons are significant, P < 0.005. Data was normalized to yeast grown in the presence of glucose without PAO (i). (G) Sec7-GFP expressing-yeast treated with PAO for 30 min. (H) Quantification of Sec7-GFP TGN localization in (G) (*, versus untreated, P < 0.05). (I) Glucose starvation of yeast co-expressing Sec7-RFP and GFP-PH^{OSBP}. (J) Quantification of Sec7-RFP TGN localization in (J). Scale bars, 2 μm. All error bars, SEM. See also Figure S3.

Figure 4. Glucose regulates PH domain binding to the TGN via pH_c. (A) Confocal micrographs of WT and Δ*reg1* yeast expressing GFP-PH^{OSBP}. Cells were glucose starved for 30 min and imaged (-Glucose) and were imaged again 10 min after re-addition of either glucose (reGlucose) or glucose plus 100 μM ebselen (reGlucose +ebselen). (B) Quantification of GFP-PH^{OSBP} TGN localization in (A) (*, $P < 0.0001$ versus +Glucose). (C) Confocal micrographs of WT and Δ*reg1* yeast expressing Arf1-GFP before and after 30 min of glucose starvation. (D) Quantification of Arf1-GFP TGN localization in (C) (*, $P < 0.001$ versus +Glucose). (E) pH_c measurements of *Tpk1-as* cells after glucose starvation for the indicated times either in the absence or presence of 1NM-PP1 (*, -Glucose versus -Glucose +1NM-PP1 at given timepoint, $P < 0.05$). (F) pH_c measurements of *Tpk1-as* cells after treatment with 100 μM ebselen for the indicated times either in the absence or presence of 1NM-PP1 (*, versus -ebselen at given timepoint, $P < 0.05$). (G) Confocal micrographs of 1NM-PP1 treated WT and *Tpk1-as* cells expressing GFP-PH^{OSBP} after glucose starvation for the indicated times. (H) Quantification of GFP-PH^{OSBP} TGN localization in (G) (*, versus WT at given timepoint, $P < 0.001$). Scale bars, 2 μm; pH_c, cytoplasmic pH; Error bars indicate SEM; except (E,F), SD. See also Figure S4.

Figure 5. Osh1 TGN localization is regulated by glucose, pH_c and PI4P. (A) Confocal micrographs of yeast cells expressing GFP-Osh1 versus GFP-$Osh1^{AA}$ (*, indicates localization to the nucleus-vacuole junction (NVJ)). (B,C) Quantification of TGN (B) and NVJ (C) localizations for GFP-Osh1 and GFP-$Osh1^{AA}$ in (A) (*, $P < 0.0001$). (D) Localization of GFP-Osh1 in WT and *pik1-104* mutants grown at 25°C versus 30°C (*, indicates localization to the NVJ). (E,F) Quantification of TGN (E) and NVJ (F) localizations for GFP-Osh1 in (D) (*, $P < 0.0001$). (G) Confocal micrographs of WT yeast expressing GFP-Osh1 and treated with 100 μM ebselen for 5min (*, indicates localization to the NVJ). (H) Quantification of GFP-Osh1 TGN-localization in (G) (*, $P < 0.0001$). (I) Confocal micrographs of WT yeast expressing GFP-Osh1

imaged 10 min after addition of 2 mM 2,4-DNP buffered at pH 7.2 or pH 6 (*, indicates localization to the NVJ). (J) Quantification of GFP-Osh1 TGN localization in (I) (*, $P < 0.0001$). (K) Confocal micrographs of GFP-Osh1-expressing WT, *pma1-007* and Δ*reg1 pma1-007* cells grown in pH 3 and pH 5 buffered medium (*, indicates localization to the NVJ). (L) Quantification of GFP-Osh1 TGN localization in (K) (*, versus pH 5, $P < 0.0001$). (M) Confocal micrographs of WT and *Δsac1* yeast expressing GFP-Osh1 before and after glucose starvation (*, indicates localization to the NVJ). (N) Quantification of GFP-Osh1 TGN localization in (M) (*, versus WT at corresponding timepoint, $P < 0.05$). Scale bars, 2 μm. All error bars indicate SEM. See also Figure S5.

Figure 6. Osh1 regulates Tat2 trafficking and tryptophan uptake. (A) Yeast spot assays of WT and Δ*osh1* yeast grown on medium supplemented with 40 μM (low Trp) or 0.3 mM (high Trp) tryptophan at 25°C. (B) Spot assays of WT and Δ*osh1* yeast over-expressing GFP-Osh1 or GFP-Osh1^{AA} grown as in (A). (C) Spot assays of *pik1-104* cells grown as in (A) but at the semi-permissive temperature of 30°C. (D) Confocal micrographs of WT and *Δosh1* mutants expressing Tat2-GFP. (E) Quantification of Tat2-GFP localization at the plasma membrane (PM) in (D) (*, $P < 0.0001$). (F) Spot assays of WT and Δ*osh1* yeast over-expressing Tat2-GFP grown as in A (empty indicates empty vector). (G) Functional enrichment for *OSH1* genetic interactions. Node size indicates statistical significance of enriched GO terms and edges indicate statistically significant associations between terms. Node colour indicates the % of aggravating or alleviating interactions in each term (50/50 indicated in white). Scale bars, 2 μm. WT, wild type. Error bars indicate SEM.

Figure 7. pH_c regulates Tat2 trafficking and tryptophan uptake. (A) Yeast spot assays with the indicated mutants grown on pH 4 buffered medium supplemented with 40 μM (low Trp) or 0.3 mM (high Trp) tryptophan at 25 °C. (B) Spot assays with the indicated mutants on pH 4 or

pH 5 buffered medium grown as in (A). (C) Confocal micrographs WT and *pma1-007* mutants expressing Tat2-GFP grown in pH 3 or pH 5 buffered medium. (D) Quantification of Tat2-GFP PM localization in (C) (*, versus pH 5, $P < 0.0001$). (E) Spot assays with WT and *pma1-007* cells overexpressing Tat2-GFP and grown as in (A) on pH 4 buffered medium. (F) Spot assays of WT and *pma1-007* cells overexpressing GFP-Osh1 or GFP-Osh1^{AA} and grown as in (A) on pH 4 buffered medium. (G) Confocal micrographs of WT yeast expressing Tat2-GFP before and after glucose starvation for the indicated times, after re-addition of glucose or re-addition of glucose in the presence of ebselen for 10 min. (H) Quantification of Tat2-GFP PM localization in (H) (*, $P < 0.05$ versus prior condition). (I) Yeast cells expressing Tat2-GFP and the late endosomal marker Snf7-RFP before and after glucose starvation. (J) Yeast cells expressing Tat2-GFP and the TGN marker Sec7-RFP before and after glucose starvation. (K) Spot assays of the indicated mutants grown on pH 4 buffered synthetic complete medium at the semi-permissive temperature of 30°C. (L) Model for pH biosensing by PI4P at the TGN and role for Osh1 in sterol-PI4P counter-transport and Tat2 trafficking. Scale bars, 2 μm. Error bars indicate SEM. WT, wild type. Cyto, cytoplasmic. PM, plasma membrane

STAR METHODS

KEY RESOURCES TABLE

See 'KEY RESOURCES TABLE' excel sheet.

LEAD CONTACT AND MATERIALS AVAILABILITY

Further information and requests for resources and reagents should be directed to and will be fulfilled by the Lead Contact, Christopher J.R. Loewen (email: christopher.loewen@ubc.ca). Plasmids and strains generated in this study are available upon request.

EXPERIMENTAL MODELS AND SUBJECT DETAILS

Yeast Strains, Plasmids, Media, Growth Conditions and Drug Treatment

Yeast strains and plasmids are described in the Key Resources Table. Yeast plasmids were generated using standard polymerase chain reaction (PCR) and cloning techniques. Yeast cells were transformed using methods involving lithium acetate: The 'Quick and Dirty Plasmid Transformation of Yeast Colonies' were used for the transformation of plasmids, while the 'High-Efficiency Transformation of Yeast' were used for the transformation of PCR products and linearized plasmid DNA (Cold Spring Harbor Protocols). The one-step PCR-based method was used to generate chromosomal integrated gene deletions and epitope-tagged proteins and confirmed by PCR (Longtine et al., 1998; Janke et al., 2004; Haruki et al., 2008). All yeast strains imaged by microscopy were grown to mid-log phase at 30 °C in liquid synthetic medium unless otherwise indicated. For glucose starvation experiments, yeast were grown in medium containing 2% glucose, pelleted, washed once, and resuspended in the same medium lacking glucose. All confocal images of Tat2-GFP were taken from cells grown in synthetic medium with 40 μM tryptophan at 25 °C. For plate assays, yeast strains used in tryptophan auxotrophy plate assays were incubated in synthetic medium with 40 μM or 0.3 mM tryptophan at 25 °C temperature for 2 days unless otherwise indicated. All pH 3 and 4 media were buffered with 50

mM sodium phosphate, while pH 5 media was buffered with 50 mM sodium succinate, and adjusted to the indicated pH with HCl and KOH. All growth assays were repeated a minimum of two times. Ebselen treatment was as previously described (Young et al., 2010); ebselen was added directly to liquid culture to obtain a final concentration of 100 µM and incubated for a minimum of 5 min. 2,4-dinitrophenol (2,4-DNP) treatment was adapted from previously described methods (Dechant et al., 2010); cultured cells were washed once in DNP buffer (25 mM HEPES, 150 mM KCl, 25 µM $CaCl_2$, 2% glucose, adjusted to the indicated pH with HCl and KOH) and resuspended in DNP buffer with 2mM 2,4-DNP. Confocal images were taken after 10 min of incubation at 30 °C. 1NM-PP1 treatment was as previously described (Aoh et al., 2013); WT and *Tpk1-as* mutants were grown in YPD and treated with 2 µM 1NM-PP1 or an equivalent amount of DMSO after growth to mid-log phase for 1 h before the 0 min time point. The cells were then treated as indicated according to the methods described above. Phenylarsine oxide (PAO) treatment involved the addition of 150 µM PAO to the designated medium for the indicated time.

METHOD DETAILS

Confocal Microscopy and Quantification of Microscopy Images

Images were captured using the Pascal Laser Scanning Microscope (Zeiss) under identical microscope settings to enable direct comparison between different treatments. The TGN localization of fluorescent-tagged proteins were quantified in the following way. ImageJ software (Schneider et al., 2012) was used to plot the pixel profile of a line drawn across a fluorescent punctate dot and the cytoplasm of a single cell. This data was then plotted in excel using a 3 pixel moving average. From this plot, the value of the peak pixel intensity of the punctate dot over the mean pixel intensity of the cytoplasm was then determined. This value was obtained for the brightest 3 punctate dots of a single confocal plane in the same cell and averaged to give a representative quantification of TGN localization for each quantified cell. The mean was then

taken from the values of all the quantified cells to give the final 'TGN / Cyto Ratio'. Quantification of the localization of GFP-tagged proteins to the PM or nucleus vacuole junction (NVJ) were performed in the same manner to obtain the 'PM / Cyto Ratio' and 'NVJ / Cyto Ratio', except that only one line was drawn and quantified per cell. The peak PM pixel intensity for each cell was averaged to obtain the 'PM intensity'. A minimum of 30 cells per treatment was quantified for all quantifications and every cell in each confocal field was counted. All experiments were repeated a minimum of two times.

Liposome binding assays

MBP-fusion proteins were expressed and purified from bacteria as previously described (Young et al., 2010). Plasmids containing MBP-fusion proteins were transformed into competent E.coli. These bacteria were then cultured in LB liquid media containing 0.2% dextrose and ampicillin (BM) at 37 °C to obtain a 4 L culture at log-phase growth of OD ~0.5. 1 mL of 1 M IPTG was then added directly to the 4 L culture and incubated at 37 °C for 4 hrs. The bacteria were then pelleted by centrifugation and frozen with liquid nitrogen. The pellets were then resuspended in Binding Buffer (25 mM Hepes pH 7.4, 150 mM KCl, 25 µM CaCl2, 1 mM DTT and 1 mM AEBSF) and homogenized by nitrogen cavitation using a pressure of 17,000 psi. The homogenate was then cleared by centrifugation, suspended with amylose resin and incubated at 4 °C for ~1 hr. The amylose resin were then washed thrice with Binding Buffer and then added to a column to elute MBP-fusion proteins with Binding Buffer containing 20 mM Maltose. Fractions containing the MBP-fusion proteins were then stored at -80 °C in 15% glycerol until needed. MBP-tagged PH^{OSBP}, $PH^{OSBP(AA)}$, PH^{Osh1}, and $PH^{Osh1(AA)}$ were then tested for binding to synthetic lipid vesicles as follows. Dioleoyl PC, dioleoyl PE, porcine brain PI4P, and porcine brain PIP2 (purchased from 'Avanti Polar Lipids, Inc.') suspended in chloroform was added to a clean glass tube at the indicated percentage where the total lipid concentration in the tube was 6.6 µmol. This mixture of lipids was then vortexed and evaporated using CO_2 gas. The lipids

were next rehydrated in 1 ml Liposome Buffer (250 mM Raffinose, 25 mM Hepes pH 7.4) and vortexed. This mixture of lipids were then formed into raffinose encapsulated liposomes through extrusion with the 'Avanti Mini-Extruder' system, using a 'Whatman PC MB 19MM .1UM filter' and 'Whatman Drain Disc 10MM PE' discs, and stored on ice until use. 53.5 µL of liposomes were added to 1 mL of Binding Buffer (25 mM Hepes pH 7.4, 150 mM KCl, 25 µM $CaCl_2$, 1 mM DTT, 1 mM AEBSF, 1 mg/mL soybean trypsin inhibitor,) and sedimented by centrifugation at 50,000 rpm for 30 min at 4°C using the 'Beckman Coulter TLA-120.2 Rotor'. The pellet was then resuspended in 250 µL of Binding Buffer, adjusted to the indicated pH, with 5 µg of protein, which resulted in a final liposome concentration of 1.4 mM and protein concentration of ~ 0.4 mM) and incubated for 30 min at room temperature. The liposomes were then pelleted and washed twice with 200 µL of the same pH Binding Buffer twice. The liposomes were then resuspended in 20 µL Sample Buffer and run on a gel and stained with Commassie Blue. Relative binding of PH^{OSBP} to pH 8 was quantified as follows: ImageJ software (Schneider et al., 2012) was used to plot the profile of the density of PH^{OSBP} for each lane (pH 6, 6.4, 6.8, 7.2, 7.6, 8) in a gel. The ratio was then taken of the density of the indicated pH versus the average density of all the lanes in the gel in order to obtain 'relative binding'. The ratio of the average relative binding at the indicated pH versus the average relative binding at pH 8 across three independent replicates was used to normalize binding relative to pH 8. All liposome binding experiments were repeated at least two times.

Arf1 in vitro binding experiments

GST-, 6xHis- and MBP-fusion proteins were expressed and purified from bacteria as previously described (Gillingham et al., 2004). Plasmids containing these fusion proteins were transformed into competent *E. coli*. These bacteria were then cultured in 2XTYE media containing ampicillin at 37 °C to obtain a 1 L culture at log-phase growth of OD ~0.6. 100 µL of 1 M IPTG was then added directly to each 1 L culture and incubated at 17 °C overnight. The bacteria were then

pelleted by centrifugation and frozen with liquid nitrogen. The pellets were then resuspended in pre-chilled AL's Buffer (25 mM Tris pH 7.4, 110 mM KCl, 5 mM Mgcl2, 1% Triton X-100, 1 mM PMSF and cOmplete Protease Inhibitor Tablets (1 per 50 mL)), dounce homogenized with 10X strokes using a 30 cm2 dounce homogenizer for each ~40 mL of cell suspension, sonicated and cleared by centrifugation. The homogenate was then split equally into three treatments; untreated, homogenate with 100 µM Guanosine 5'-diphosphate (GDP) added to it, and homogenate with 100 µM Guanosine 5'-[β,γ-imido]triphosphate (GTP-γ-S) added to it. These homogenates were then incubated for 5 min at 4 °C to ensure the nucleotides had locked. Glutathione Sepharose Beads (GE Healthcare: 17-0756-01) were then added to each GST-fusion protein (bait) homogenate and incubated for 30 min at 4 °C. The beads were then washed 2X with AL's Buffer containing the relevant nucleotide for each treatment. The 6xHis- and MBP-fusion proteins (prey) homogenates containing the relevant nucleotide were then added to the indicated bait bead and incubated for 1 hr at 4 °C. The beads were then washed 5X with AL's Buffer containing the relevant nucleotide. The beads were then eluted through a column with 1X Sample Buffer containing 10% β-mercaptoethanol preheated to 90 °C. The samples were then analyzed on SDS-PAGE gels stained with Coomassie blue stain.
All GST- binding experiments were repeated at least three times.

Measurement of pH_c

pH_c measurements were performed as described previously described (Young et al., 2010). Yeast strains expressing P*ACT*-pHluorin were cultured at 30 °C in low fluorescence medium (synthetic defined medium without riboflavin or folic acid, 1 mM inositol, 2% glucose), buffered with 25 mM citrate to pH 5.0 in CELLSTAR black polystyrene clear-bottomed 96-well microtiter plates. At mid-log phase, fluorescence emission was determined in a SpectraMax Gemini XS spectrofluorometer (Molecular Devices) at 512 nm after excitation at 390 nm and 470 nm. Both

intensities were corrected for the background fluorescence of a control strain (empty vector) subjected to identical experimental conditions. The ratio of the two intensities was related to that of a calibration curve of cells permeabilized with digitonin (100 µg/ml for 10 min) and resuspended in buffers with pH between 5.0 and 9.0. Each experiment represents the average and standard deviation of three independent replicates.

In vivo phosphoinositide analysis

Cellular phosphoinositide levels were measured as previously described (Audhya et al., 2000). Yeast were grown to early log phase of ~0.6 at 30 °C in synthetic medium lacking inositol (IFM). In the case of phosphoinositide measurements of WT compared to *pma1-007* and *Δosh1* mutants, all IFM was buffered to pH 4. *Δsac1* mutants were grown in unbuffered IFM, pelleted, washed, and then resuspended in unbuffered IFM with or without 2% glucose. For WT cells treated with 2,4-DNP, cells were then pelleted, washed, and resuspended in 1 mL DNP buffer at the indicated pH. Following this, cells were then treated with 2 mM 2,4-DNP, incubated for 10 min at 30 °C, and then washed with DNP buffer. 5 OD_{600} of cells were pelleted, washed, and resuspended in 450 µL of the previously designated IFM and then incubated at room temperature for 15 min. 50 uL of 3H-myoinositol (1 µL = 1 uCi) (PerkinElmer) was added to each culture of cells and incubated at room temperature for 1 hr. The cultures were then added to a pre-chilled 1.5 mL eppendorf tube containing 500 µL of 9% perchloric acid (PCA) with ~400 µL of glass beads, inverted to mix and incubated on ice for 5 min. The tube was then vortexed for 5 min at top speed and its lysates were transferred to a new eppendorf tube. The lysate was then centrifuged for 10 min at 4 °C at top speed and its supernatant was then aspirated out. The pellet was then resuspended in pre-chilled 100 mM EDTA and vortexed for 1 min and then spinned and aspirated as before. The pellet was then resuspended in 50 µL ddH20 by sonication. The suspension was then transferred to a new eppendorf tube containing 1 mL of Deacylation Reagent (4.6 mL 100% methanol, 2.6 mL 40% methylamine, 1.1 mL 100% 1-

butanol and 1.6 mL ddH20. The suspension was then vortexed and sonicated again, let sit at room temperature for 30 min, vortexed and placed in a 53 °C heating block for 50 min. The samples were then completely dried using a hotroom speedvac, resuspended in 500 µL ddH20, sonicated to complete dispersion, let sit at room temperature for 30 min and completely dried again with the speedvac. The dried pellet was then resuspended in 300 µL ddH20 by sonication and incubated at room temperature for 30 min. 300 µL of Extraction Reagent (4 mL 100% 1-butanol, 800 µL 100% ethyl ether and 200 µL 100% ethyl formate) was then added and vortexed at top speed for 1 min. The samples were then centrifuged for 3 min at top speed to separate the phases. The bottom aqueous layer was collected in a new tube without disturbing the interface. Phase separation and collection of the bottom layer were repeated twice more to ensure purity of the sample. The samples were then dried in a speedvac, resuspended in 25 µL of ddH20 by sonication and centrifuged to collect the supernatant used as the final sample for HPLC (high-performance liquid chromatography) analysis. HPLC was performed on a Beckman System Gold using a 25-cm Partisil 5 SAX column (Whatman). The column was developed with a gradient of (NH4)2-PO4, pH 3.8, generated as follows; the flow rate was 1.0 mL/min. The column was calibrated using 32P-labeled glycerophosphoinositols generated in an in vitro PI 3-kinase assay. In addition, each sample was spiked with unlabeled AMP and ADP, and their elution was minotred with a UV absorbance detector to assess column performance. Fractions eluting from the HPLC column were collected every 0.66 min and counted in a scintillation counter (LC6000IC; Beckman Instruments) using Cytoscint (ICN Radiochemicals) scintillation fluid. Each experiment represents the average and standard deviation of three technical replicates.

Hydrogen deuterium exchange (HDX)

The PH domain of OSBP was diluted into three different storage buffers at pH-6.4, 6.8, and 7.2 (20 mM Hepes, 100 mM NaCl, and 2mM TCEP), and was concentrated and buffer exchanged

using an Amicon 50K centrifugal filter (Millipore) to a final concentration of 20 μM. Deuterium exchange experiments were initiated by a dilution of protein into deuterated buffer matching the protein buffer pH (20 mM Hepes, 100 mM NaCl, and 2 mM TCEP in 96% D_2O) to a final concentration of 80% D_2O. On exchange hydrogen deuterium exchange experiments were carried out for three different timepoints (3, 30, and 300 seconds of on exchange). The reaction was quenched by the addition of formic acid to a final concentration of 1% and a final protein concentration of 3 μM. The protein was then immediately snap frozen on liquid nitrogen. All experiments were carried out in triplicate at every timepoint.

Mass spectrometry

Intact protein HDX measurements were carried out on a Bruker 12T Apex-Qe hybrid FT-ICR mass spectrometer (Bruker Daltonics, Billerica, MA, USA). Specific instrumental settings used have been described previously (Pan et al., 2009). Protein aliquots (15 μL) were quickly thawed on ice and instantly injected onto the HPLC column (C4, 30×2 mm, Phenomenex Inc., Torrance, CA, USA) and analyzed by LC-MS (Pan and Borchers, 2014). The samples were manually injected, with the column eluent diverted from the ESI source for the first two minutes to prevent salts from entering the instrument. To minimize back-exchange, the column, injector (Rheodyne Model 7125, loop volume 20 μL), and coiled solvent delivery lines were all embedded in an ice bath. The mobile phase was 0.1% formic acid (A) and acetonitrile with 0.1% formic acid (B). The protein was eluted with a linear binary solvent gradient from 5-60% B in 5 min. The time-dependent change in protein deuteration level was found to be negligible during the elution-time window. The intact protein HDX data were processed using the Bruker Data Analysis software (version 4.0). Normalization of deuterium incorporation to the level at pH-7.2 was carried out according to the methods of (Coales et al., 2010).

QUANTIFICATION AND STATISTICAL ANALYSIS

Statistical significance of quantified confocal images and pH measurement experiments were tested using two-tailed *t*-tests. Significance for all quantifications were at a minimum of $P < 0.05$. For figures where *n* was 3 or less, SD was used over SEM to more accurately reflect the variance of the data. Otherwise all other error bars indicate SEM.

DATA AND CODE AVAILABILITY

Datasets associated with this study are provided in Tables S1 (Genetic Interactions for OSH1. Related to Figure 6) and S2 (Results of ClueGO Analysis for *OSH1* Genetic Interactions. Related to Figure 6).

SUPPLEMENTAL TABLES

Table S1: Genetic Interactions for OSH1. Related to Figure 6.

Table S2: Results of ClueGO Analysis for *OSH1* Genetic Interactions. Related to Figure 6.

Table S3: Yeast strains used in this study. Related to STAR methods

References

Aoh, Q.L., Graves, L.M., and Duncan, M.C. (2011). Glucose regulates clathrin adaptors at the trans-Golgi network and endosomes. Mol Biol Cell *22*, 3671–3683.

Aoh, Q.L., Hung, C.-W., and Duncan, M.C. (2013). Energy metabolism regulates clathrin adaptors at the trans-Golgi network and endosomes. Mol Biol Cell *24*, 832–847.

Audhya, A., Foti, M., and Emr, S.D. (2000). Distinct roles for the yeast phosphatidylinositol 4-kinases, Stt4p and Pik1p, in secretion, cell growth, and organelle membrane dynamics. Molecular Biology of the Cell *11*, 2673–2689.

Barylko, B., Gerber, S.H., Binns, D.D., Grichine, N., Khvotchev, M., Sudhof, T.C., and Albanesi, J.P. (2001). A novel family of phosphatidylinositol 4-kinases conserved from yeast to humans. J. Biol. Chem. *276*, 7705–7708.

Beck, T., Schmidt, A., and Hall, M.N. (1999). Starvation induces vacuolar targeting and degradation of the tryptophan permease in yeast. J. Cell Biol. *146*, 1227–1238.

Beh, C.T., Cool, L., Phillips, J., and Rine, J. (2001). Overlapping functions of the yeast oxysterol-binding protein homologues. Genetics *157*, 1117–1140.

Chan, G., Hardej, D., Santoro, M., Lau-Cam, C., and Billack, B. (2007). Evaluation of the antimicrobial activity of ebselen: role of the yeast plasma membrane H+-ATPase. J. Biochem. Mol. Toxicol. *21*, 252–264.

Chung, J., Torta, F., Masai, K., Lucast, L., Czapla, H., Tanner, L.B., Narayanaswamy, P., Wenk, M.R., Nakatsu, F., and De Camilli, P. (2015). INTRACELLULAR TRANSPORT. PI4P/phosphatidylserine countertransport at ORP5- and ORP8-mediated ER-plasma membrane contacts. Science *349*, 428–432.

Coales, S.J., E, S.Y., Lee, J.E., Ma, A., Morrow, J.A., and Hamuro, Y. (2010). Expansion of time window for mass spectrometric measurement of amide hydrogen/deuterium exchange reactions. Rapid Commun. Mass Spectrom. *24*, 3585–3592.

Cosson, P., de Curtis, I., Pouyssegur, J., Griffiths, G., and Davoust, J. (1989). Low cytoplasmic pH inhibits endocytosis and transport from the trans-Golgi network to the cell surface. J. Cell Biol. *108*, 377–387.

Costanzo, M., VanderSluis, B., Koch, E.N., Baryshnikova, A., Pons, C., Tan, G., Wang, W., Usaj, M., Hanchard, J., Lee, S.D., et al. (2016). A global genetic interaction network maps a wiring diagram of cellular function. Science *353*, aaf1420–aaf1420.

Daboussi, L., Costaguta, G., and Payne, G.S. (2012). Phosphoinositide-mediated clathrin adaptor progression at the trans-Golgi network. Nat. Cell Biol. *14*, 239–248.

Daboussi, L., Costaguta, G., Ghukasyan, R., and Payne, G.S. (2017). Conserved role for Gga proteins in phosphatidylinositol 4-kinase localization to the trans-Golgi network. Pnas *114*, 3433–3438.

Dechant, R., Binda, M., Lee, S.S., Pelet, S., Winderickx, J., and Peter, M. (2010). Cytosolic pH is a second messenger for glucose and regulates the PKA pathway through V-ATPase. Embo J. *29*, 2515–2526.

Dechant, R., Saad, S., Ibáñez, A.J., and Peter, M. (2014). Cytosolic pH regulates cell growth through distinct GTPases, Arf1 and Gtr1, to promote Ras/PKA and TORC1 activity. Mol. Cell *55*, 409–421.

Demmel, L., Beck, M., Klose, C., Schlaitz, A.-L., Gloor, Y., Hsu, P.P., Havlis, J., Shevchenko, A., Krause, E., Kalaidzidis, Y., et al. (2008). Nucleocytoplasmic shuttling of the Golgi phosphatidylinositol 4-kinase Pik1 is regulated by 14-3-3 proteins and coordinates Golgi function with cell growth. Mol Biol Cell *19*, 1046–1061.

Fairn, G.D., Curwin, A.J., Stefan, C.J., and McMaster, C.R. (2007). The oxysterol binding protein Kes1p regulates Golgi apparatus phosphatidylinositol-4-phosphate function. Pnas *104*, 15352–15357.

Faulhammer, F., Kanjilal-Kolar, S., Knödler, A., Lo, J., Lee, Y., Konrad, G., and Mayinger, P. (2007). Growth control of Golgi phosphoinositides by reciprocal localization of sac1 lipid phosphatase and pik1 4-kinase. Traffic *8*, 1554–1567.

Faulhammer, F., Konrad, G., Brankatschk, B., Tahirovic, S., Knödler, A., and Mayinger, P. (2005). Cell growth-dependent coordination of lipid signaling and glycosylation is mediated by interactions between Sac1p and Dpm1p. J. Cell Biol. *168*, 185–191.

Ferguson, K.M., Lemmon, M.A., Schlessinger, J., and Sigler, P.B. (1995). Structure of the high affinity complex of inositol trisphosphate with a phospholipase C pleckstrin homology domain. Cell *83*, 1037–1046.

Foti, M., Audhya, A., and Emr, S.D. (2001). Sac1 lipid phosphatase and Stt4 phosphatidylinositol 4-kinase regulate a pool of phosphatidylinositol 4-phosphate that functions in the control of the actin cytoskeleton and vacuole morphology. Mol Biol Cell *12*, 2396–2411.

Gloor, Y., Schöne, M., Habermann, B., Ercan, E., Beck, M., Weselek, G., Müller-Reichert, T., and Walch-Solimena, C. (2010). Interaction between Sec7p and Pik1p: the first clue for the regulation of a coincidence detection signal. Eur. J. Cell Biol. *89*, 575–583.

Godi, A., Di Campli, A., Konstantakopoulos, A., Di Tullio, G., Alessi, D.R., Kular, G.S., Daniele, T., Marra, P., Lucocq, J.M., and De Matteis, M.A. (2004). FAPPs control Golgi-to-cell-surface membrane traffic by binding to ARF and PtdIns(4)P. Nat. Cell Biol. *6*, 393–404.

Isom, D.G., Sridharan, V., Baker, R., Clement, S.T., Smalley, D.M., and Dohlman, H.G. (2013). Protons as Second Messenger Regulators of G Protein Signaling. Molecular Cell *51*, 531–538.

Jiang, B., Brown, J.L., Sheraton, J., Fortin, N., and Bussey, H. (1994). A new family of yeast genes implicated in ergosterol synthesis is related to the human oxysterol binding protein. Yeast *10*, 341–353.

Kooijman, E.E., King, K.E., Gangoda, M., and Gericke, A. (2009). Ionization properties of phosphatidylinositol polyphosphates in mixed model membranes. Biochemistry *48*, 9360–9371.

Kooijman, E.E., Tieleman, D.P., Testerink, C., Munnik, T., Rijkers, D.T., Burger, K.N., and de Kruijff, B. (2007). An electrostatic/hydrogen bond switch as the basis for the specific interaction of phosphatidic acid with proteins. J. Biol. Chem. *282*, 11356–11364.

Kvam, E., and Goldfarb, D.S. (2004). Nvj1p is the outer-nuclear-membrane receptor for oxysterol-binding protein homolog Osh1p in Saccharomyces cerevisiae. J Cell Sci *117*, 4959–4968.

Kvam, E., and Goldfarb, D.S. (2006). Structure and function of nucleus-vacuole junctions: outer-nuclear-membrane targeting of Nvj1p and a role in tryptophan uptake. J Cell Sci *119*, 3622–3633.

Lemmon, M.A. (2008). Membrane recognition by phospholipid-binding domains. Nat. Rev. Mol. Cell Biol. *9*, 99–111.

Levine, T.P., and Munro, S. (2001). Dual targeting of Osh1p, a yeast homologue of oxysterol-binding protein, to both the Golgi and the nucleus-vacuole junction. Mol Biol Cell *12*, 1633–1644.

Levine, T.P., and Munro, S. (2002). Targeting of Golgi-specific pleckstrin homology domains involves both PtdIns 4-kinase-dependent and -independent components. Curr. Biol. *12*, 695–704.

Li, Z., Vizeacoumar, F.J., Bahr, S., Li, J., Warringer, J., Vizeacoumar, F.S., Min, R., VanderSluis, B., Bellay, J., Devit, M., et al. (2011). Systematic exploration of essential yeast gene function with temperature-sensitive mutants. Nat. Biotechnol. *29*, 361–367.

Liu, L.-K., Choudhary, V., Toulmay, A., and Prinz, W.A. (2017). An inducible ER-Golgi tether facilitates ceramide transport to alleviate lipotoxicity. The Journal of Cell Biology *216*, 131–147.

Loewen, C.J., Gaspar, M.L., Jesch, S.A., Delon, C., Ktistakis, N.T., Henry, S.A., and Levine, T.P. (2004). Phospholipid metabolism regulated by a transcription factor sensing phosphatidic acid. Science *304*, 1644–1647.

Loewen, C.J., Roy, A., and Levine, T.P. (2003). A conserved ER targeting motif in three families of lipid binding proteins and in Opi1p binds VAP. Embo J. *22*, 2025–2035.

Manik, M.K., Yang, H., Tong, J., and Im, Y.J. (2017). Structure of Yeast OSBP-Related Protein Osh1 Reveals Key Determinants for Lipid Transport and Protein Targeting at the Nucleus-Vacuole Junction. Structure *25*, 617–629.e3.

Marcireau, C., Guilloton, M., and Karst, F. (1990). In vivo effects of fenpropimorph on the yeast Saccharomyces cerevisiae and determination of the molecular basis of the antifungal property. Antimicrob. Agents Chemother. *34*, 989–993.

Martínez-Muñoz, G.A., and Kane, P. (2008). Vacuolar and plasma membrane proton pumps collaborate to achieve cytosolic pH homeostasis in yeast. J. Biol. Chem. *283*, 20309–20319.

Mesmin, B., Bigay, J., Moser von Filseck, J., Lacas-Gervais, S., Drin, G., and Antonny, B. (2013). A four-step cycle driven by PI(4)P hydrolysis directs sterol/PI(4)P exchange by the ER-Golgi tether OSBP. Cell *155*, 830–843.

Moser von Filseck, J., Čopič, A., Delfosse, V., Vanni, S., Jackson, C.L., Bourguet, W., and Drin, G. (2015). INTRACELLULAR TRANSPORT. Phosphatidylserine transport by ORP/Osh proteins is driven by phosphatidylinositol 4-phosphate. Science *349*, 432–436.

Orij, R., Urbanus, M.L., Vizeacoumar, F.J., Giaever, G., Boone, C., Nislow, C., Brul, S., and Smits, G.J. (2012). Genome-wide analysis of intracellular pH reveals quantitative control of cell division rate by pH(c) in Saccharomyces cerevisiae. Genome Biol. *13*, R80.

Pan, J., and Borchers, C.H. (2014). Top-down mass spectrometry and hydrogen/deuterium exchange for comprehensive structural characterization of interferons: implications for biosimilars. Proteomics *14*, 1249–1258.

Pan, J., Han, J., Borchers, C.H., and Konermann, L. (2009). Hydrogen/deuterium exchange mass spectrometry with top-down electron capture dissociation for characterizing structural transitions of a 17 kDa protein. J. Am. Chem. Soc. *131*, 12801–12808.

Peters, L.Z., Hazan, R., Breker, M., Schuldiner, M., and Ben-Aroya, S. (2013). Formation and dissociation of proteasome storage granules are regulated by cytosolic pH. The Journal of Cell Biology *201*, 663–671.

Raychaudhuri, S., and Prinz, W.A. (2010). The diverse functions of oxysterol-binding proteins. Annu. Rev. Cell Dev. Biol. *26*, 157–177.

Richardson, B.C., Halaby, S.L., Gustafson, M.A., and Fromme, J.C. (2016). The Sec7 N-terminal regulatory domains facilitate membrane-proximal activation of the Arf1 GTPase. eLife Sciences *5*, e12411.

Roy, A., and Levine, T.P. (2004). Multiple pools of PtdIns 4-phosphate detected using the pleckstrin homology domain of Osh2p. J. Biol. Chem.

Schmidt, A., Hall, M.N., and Koller, A. (1994). Two FK506 resistance-conferring genes in Saccharomyces cerevisiae, TAT1 and TAT2, encode amino acid permeases mediating tyrosine and tryptophan uptake. *14*, 6597–6606.

Schneider, C.A., Rasband, W.S., and Eliceiri, K.W. (2012). NIH Image to ImageJ: 25 years of image analysis. Nat. Methods *9*, 671–675.

Stefan, C.J., Manford, A.G., Baird, D., Yamada-Hanff, J., Mao, Y., and Emr, S.D. (2011). Osh Proteins Regulate Phosphoinositide Metabolism at ER-Plasma Membrane Contact Sites. Cell *144*, 389–401.

Stolz, J., and Sauer, N. (1999). The fenpropimorph resistance gene FEN2 from Saccharomyces cerevisiae encodes a plasma membrane H+-pantothenate symporter. J. Biol. Chem. *274*, 18747–18752.

Tong, A.H., and Boone, C. (2006). Synthetic genetic array analysis in Saccharomyces cerevisiae. Methods Mol. Biol. *313*, 171–192.

Tong, A.H., Evangelista, M., Parsons, A.B., Xu, H., Bader, G.D., Page, N., Robinson, M., Raghibizadeh, S., Hogue, C.W., Bussey, H., et al. (2001). Systematic genetic analysis with ordered arrays of yeast deletion mutants. Science *294*, 2364–2368.

Toulmay, A., and Prinz, W.A. (2012). A conserved membrane-binding domain targets proteins to organelle contact sites. Journal of Cell Science *125*, 49–58.

Umebayashi, K., and Nakano, A. (2003). Ergosterol is required for targeting of tryptophan permease to the yeast plasma membrane. J. Cell Biol. *161*, 1117–1131.

van Paridon, P.A., de Kruijff, B., Ouwerkerk, R., and Wirtz, K.W. (1986). Polyphosphoinositides undergo charge neutralization in the physiological pH range: a 31P-NMR study. Biochim. Biophys. Acta *877*, 216–219.

Wiedemann, C., Schafer, T., and Burger, M.M. (1996). Chromaffin granule-associated phosphatidylinositol 4-kinase activity is required for stimulated secretion. Embo J. *15*, 2094–2101.

Young, B.P., Shin, J.J.H., Orij, R., Chao, J.T., Li, S.C., Guan, X.L., Khong, A., Jan, E., Wenk, M.R., Prinz, W.A., et al. (2010). Phosphatidic acid is a pH biosensor that links membrane biogenesis to metabolism. Science *329*, 1085–1088.

KEY RESOURCES TABLE

REAGENT or RESOURCE	SOURCE	IDENTIFIER
Chemicals, Peptides, and Recombinant Proteins		
Ebselen	Cayman Chemical	#70530
2,4-Dinitrophenol	Sigma-Aldrich	24dinitrophenol184115128511
Phenylarsine Oxide	Sigma-Aldrich	P3075
Dioleoyl PC (C16-18:1)	Avanti Polar Lipids	#878112
Dioleoyl PE (C16-18:1)	Avanti Polar Lipids	#850757
Porcine brain PI(4)P	Avanti Polar Lipids	#840045
Porcine brain PI(4,5)P2	Avanti Polar Lipids	#840046
Guanosine 5'-diphosphate sodium salt (GDP)	Sigma-Aldrich	G7127
Guanosine 5’-[β,γ-imido]triphosphate trisodium salt hydrate (GTP-γ-S)	Sigma-Aldrich	G0635
3H-myoinositol	PerkinElmer	NET1168001MC
1NM-PP1	Sigma-Aldrich	529581

Experimental Models: Organisms/Strains - See Supplemental Table 3		
Recombinant DNA		
Empty vector containing a PHO5 promoter in CEN/URA3 (pRS416)	Loewen et al., 2004	pRS416
GFP, Osh1 under control of PHO5 promoter in CEN/URA3 vector (pTL310)	Loewen et al., 2003	GFP-Osh1
GFP, Osh1(280-384 aa) under control of PHO5 promoter in CEN/URA3 vector (pRS416)	This paper	GFP-PHOsh1
GFP, Osh1(280-384 aa, K289A, K290A) under control of PHO5 promoter in CEN/URA3 vector (pRS416)	This paper	GFP-PHOsh1AA
GFP, OSBP(75-188 aa) under control of PHO5 promoter in CEN/URA3 vector (pRS416)	This paper	GFP-PHOSBP
GFP, OSBP(75-188 aa, R107A, R108A) under control of PHO5 promoter in CEN/URA3 vector (pRS416)	This paper	GFP-PHOSBPAA
GFP, PHOsh2 (169 aa = 256–424 aa) ; VNSKL linker, PHOsh2 repeat, GFP under control of PHO5 promoter in CEN/URA3 vector (pRS416)	Roy & Levine, 2004	GFP-PHOsh2-dimer
Tat2(3.6-kb PstI-EcoRI fragment), GFP in YCplac33 vector to generate pKU76 (YCpTAT2-GFP)	Umebayashi & Nakano, 2003	TAT2-GFP

TRP1 Sec7ΔN-RFP under control of CMV promoter in a vector used for linearized integration into the yeast genome (pFF7)	Faulhammer et al., 2007	Sec7-RFP
MBP, Osh1(280-384 aa) for bacterial expression in pMAL-c2e vector	This paper	MBP-PHOsh1
MBP, Osh1(280-384 aa, K289A, K290A) for bacterial expression in pMAL-c2e vector	This paper	MBP-PHOsh1AA
MBP, OSBP(75-188 aa) for bacterial expression in pMAL-c2e vector	This paper	MBP-PHOSBP

Figure 2

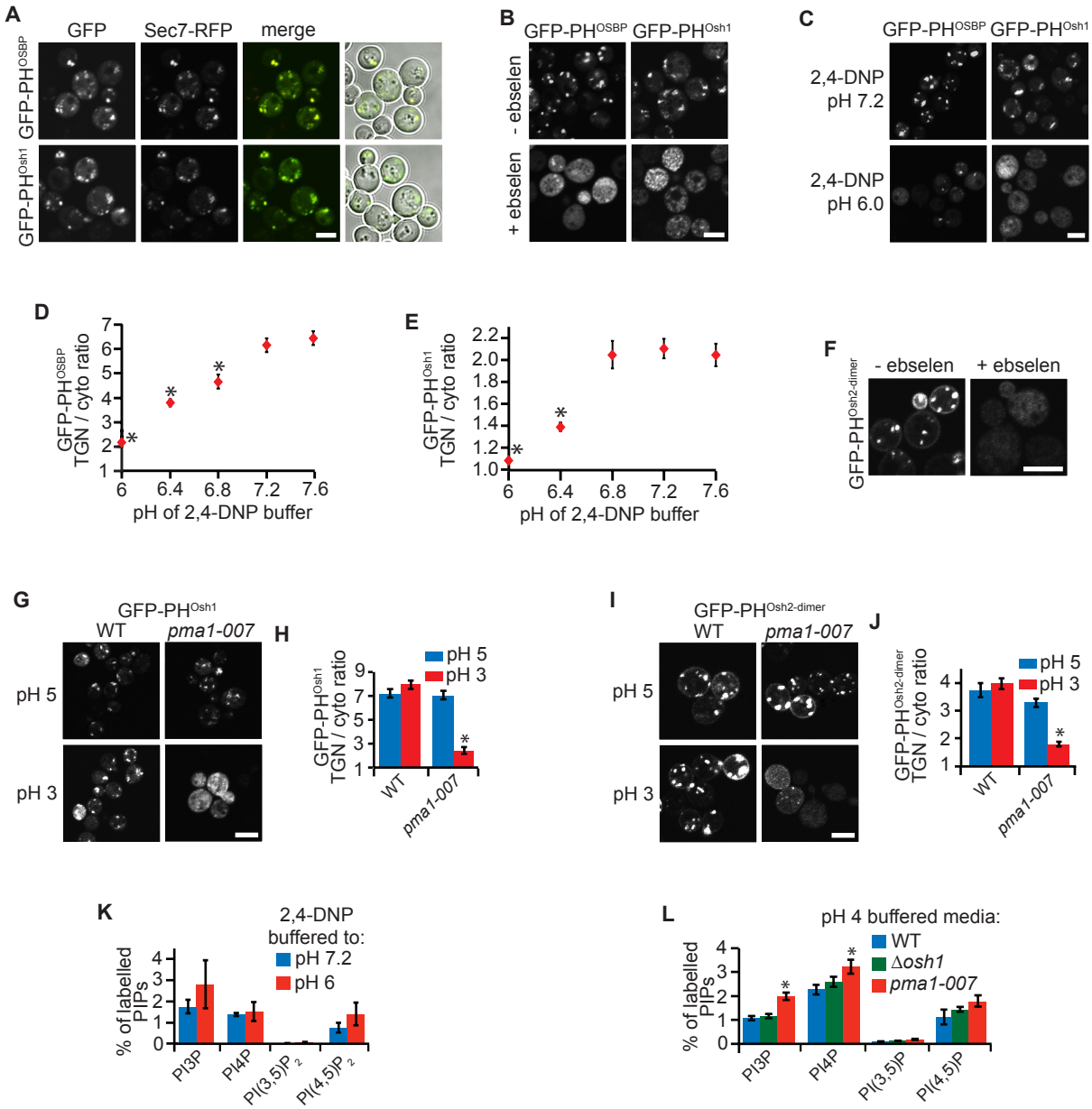
A
GFP
Sec7-RFP
merge
GFP-PHOSBP
GFP-PHOsh1
B
GFP-PHOSBP
GFP-PHOsh1
- ebselen
+ ebselen
C
GFP-PHOSBP
GFP-PHOsh1
2,4-DNP pH 7.2
2,4-DNP pH 6.0
D
GFP-PHOSBP TGN / cyto ratio
pH of 2,4-DNP buffer
E
GFP-PHOsh1 TGN / cyto ratio
pH of 2,4-DNP buffer
F
GFP-PHOsh2-dimer
- ebselen
+ ebselen
G
GFP-PHOsh1
WT
pma1-007
pH 5
pH 3
H
GFP-PHOsh1 TGN / cyto ratio
pH 5
pH 3
WT
pma1-007
I
GFP-PHOsh2-dimer
WT
pma1-007
pH 5
pH 3
J
GFP-PHOsh2-dimer TGN / cyto ratio
pH 5
pH 3
WT
pma1-007
K
2,4-DNP buffered to:
pH 7.2
pH 6
% of labelled PIPs
PI3P
PI4P
PI(3,5)P2
PI(4,5)P2
L
pH 4 buffered media:
WT
Δosh1
pma1-007
% of labelled PIPs
PI3P
PI4P
PI(3,5)P
PI(4,5)P

Figure 3

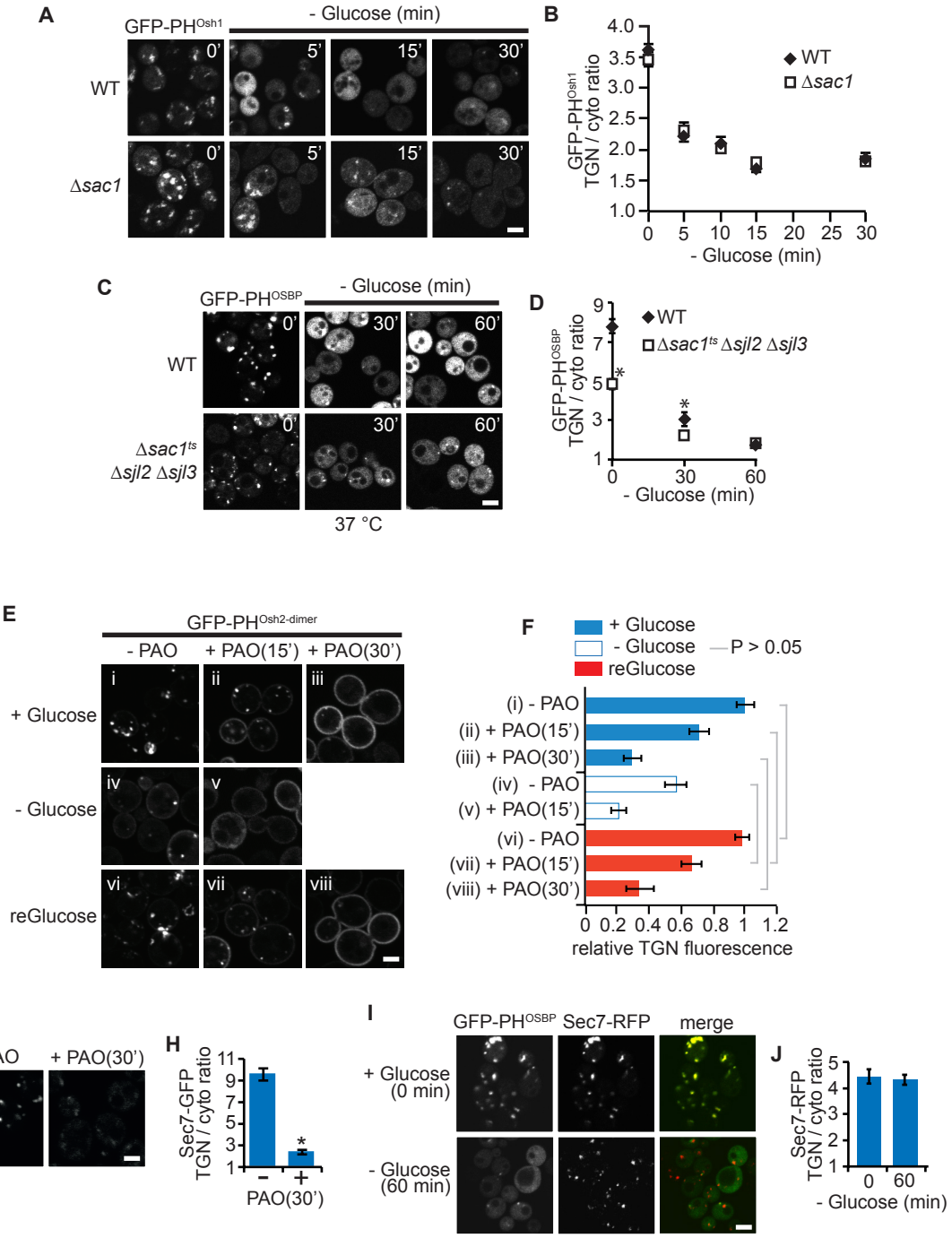
A
GFP-PHOsh1
- Glucose (min)
WT
Δsac1
0'
5'
15'
30'
B
GFP-PHOsh1 TGN / cyto ratio
WT
Δsac1
- Glucose (min)
C
GFP-PHOSBP
WT
Δsac1ts Δsjl2 Δsjl3
0'
30'
60'
37 °C
D
GFP-PHOSBP TGN / cyto ratio
WT
Δsac1ts Δsjl2 Δsjl3
- Glucose (min)
E
GFP-PHOsh2-dimer
- PAO
+ PAO(15')
+ PAO(30')
+ Glucose
- Glucose
reGlucose
i
ii
iii
iv
v
vi
vii
viii
F
+ Glucose
- Glucose
reGlucose
P > 0.05
(i) - PAO
(ii) + PAO(15')
(iii) + PAO(30')
(iv) - PAO
(v) + PAO(15')
(vi) - PAO
(vii) + PAO(15')
(viii) + PAO(30')
relative TGN fluorescence
G
- PAO
+ PAO(30')
Sec7-GFP
H
Sec7-GFP TGN / cyto ratio
PAO(30')
I
GFP-PHOSBP
Sec7-RFP
merge
+ Glucose (0 min)
- Glucose (60 min)
J
Sec7-RFP TGN / cyto ratio
- Glucose (min)

Figure 4

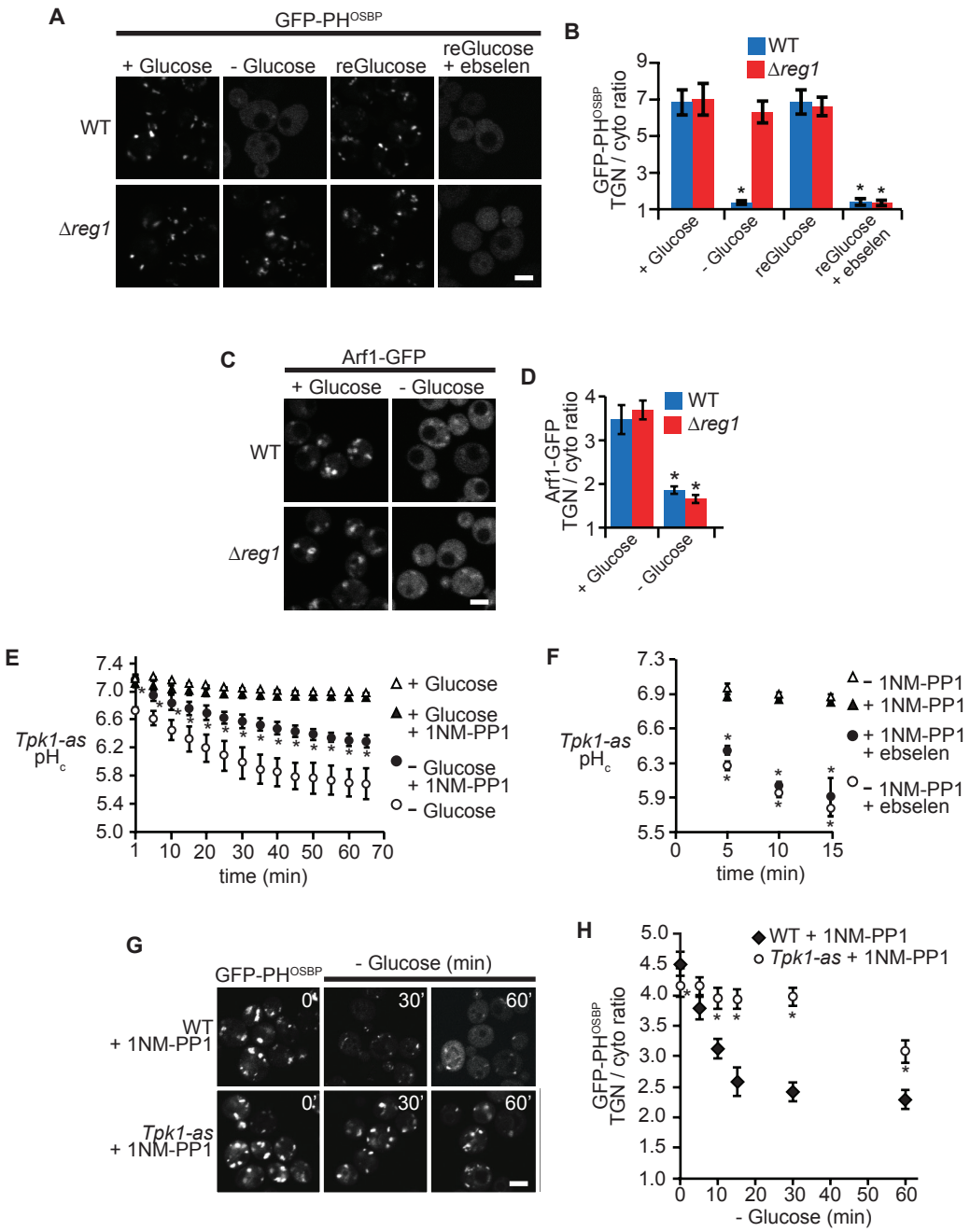
A
GFP-PH^OSBP
+ Glucose
- Glucose
reGlucose
reGlucose + ebselen
WT
Δreg1
B
WT
Δreg1
GFP-PH^OSBP TGN / cyto ratio
+ Glucose
- Glucose
reGlucose
reGlucose + ebselen
C
Arf1-GFP
+ Glucose
- Glucose
WT
Δreg1
D
WT
Δreg1
Arf1-GFP TGN / cyto ratio
+ Glucose
- Glucose
E
Tpk1-as pH_c
+ Glucose
+ Glucose + 1NM-PP1
- Glucose + 1NM-PP1
- Glucose
time (min)
F
Tpk1-as pH_c
- 1NM-PP1
+ 1NM-PP1
+ 1NM-PP1 + ebselen
- 1NM-PP1 + ebselen
time (min)
G
GFP-PH^OSBP
- Glucose (min)
WT + 1NM-PP1
Tpk1-as + 1NM-PP1
0'
30'
60'
H
WT + 1NM-PP1
Tpk1-as + 1NM-PP1
GFP-PH^OSBP TGN / cyto ratio
- Glucose (min)

Figure 5

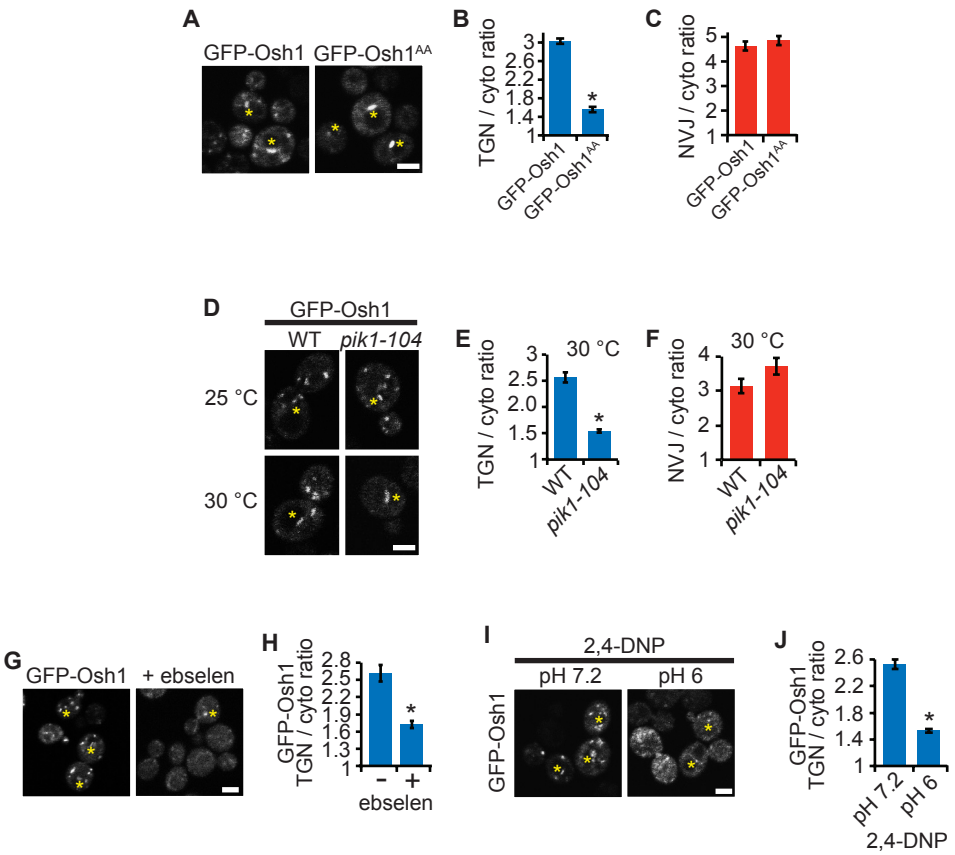
A
GFP-Osh1
GFP-Osh1AA
B
TGN / cyto ratio
GFP-Osh1
GFP-Osh1AA
C
NVJ / cyto ratio
GFP-Osh1
GFP-Osh1AA
D
GFP-Osh1
WT
pik1-104
25 °C
30 °C
E
30 °C
TGN / cyto ratio
WT
pik1-104
F
30 °C
NVJ / cyto ratio
WT
pik1-104
G
GFP-Osh1
+ ebselen
H
GFP-Osh1
TGN / cyto ratio
-
+
ebselen
I
2,4-DNP
pH 7.2
pH 6
GFP-Osh1
J
GFP-Osh1
TGN / cyto ratio
pH 7.2
pH 6
2,4-DNP
K
GFP-Osh1
WT
pma1-007
Δreg1
pma1-007
pH 5
pH 3
L
pH 5
pH 3
GFP-Osh1
TGN / cyto ratio
WT
pma1-007
Δreg1
pma1-007
M
GFP-Osh1
- Glucose (min)
WT
Δsac1
0'
5'
15'
30'
N
WT
Δsac1
GFP-Osh1
TGN / cyto ratio
- Glucose (min)

Figure 6

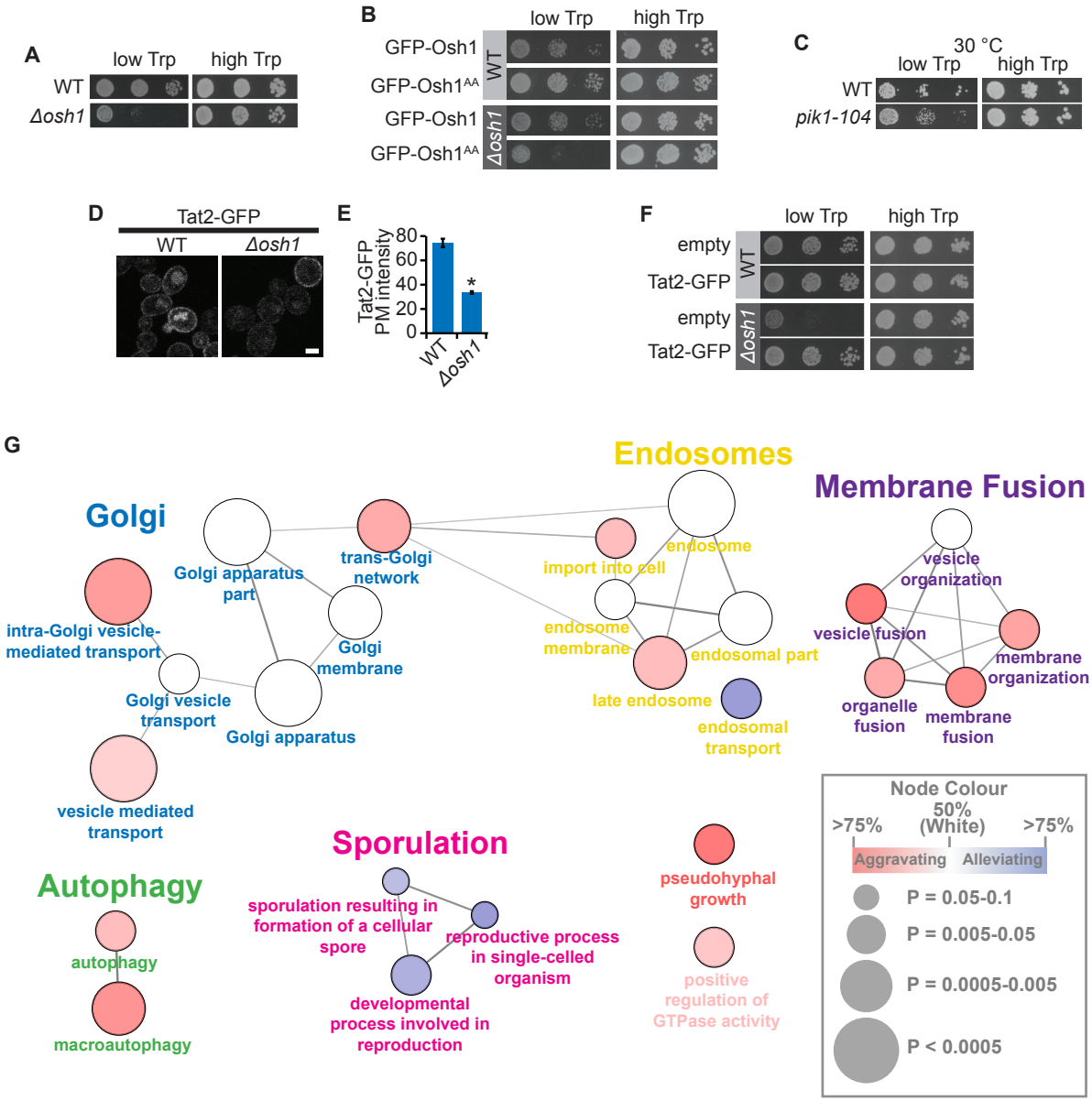
A
low Trp
high Trp
WT
Δosh1
B
low Trp
high Trp
GFP-Osh1
GFP-Osh1AA
GFP-Osh1
GFP-Osh1AA
WT
Δosh1
C
30 °C
low Trp
high Trp
WT
pik1-104
D
Tat2-GFP
WT
Δosh1
E
Tat2-GFP PM intensity
80
60
40
20
0
*
WT
Δosh1
F
low Trp
high Trp
empty
Tat2-GFP
empty
Tat2-GFP
WT
Δosh1
G
Endosomes
Membrane Fusion
Golgi
Golgi apparatus part
trans-Golgi network
intra-Golgi vesicle-mediated transport
Golgi membrane
Golgi vesicle transport
Golgi apparatus
vesicle mediated transport
import into cell
endosome
endosome membrane
endosomal part
late endosome
endosomal transport
vesicle organization
vesicle fusion
membrane organization
organelle fusion
membrane fusion
Node Colour
50% (White)
>75%
>75%
Aggravating
Alleviating
P = 0.05-0.1
P = 0.005-0.05
P = 0.0005-0.005
P < 0.0005
Sporulation
sporulation resulting in formation of a cellular spore
reproductive process in single-celled organism
developmental process involved in reproduction
Autophagy
autophagy
macroautophagy
pseudohyphal growth
positive regulation of GTPase activity

Figure 7

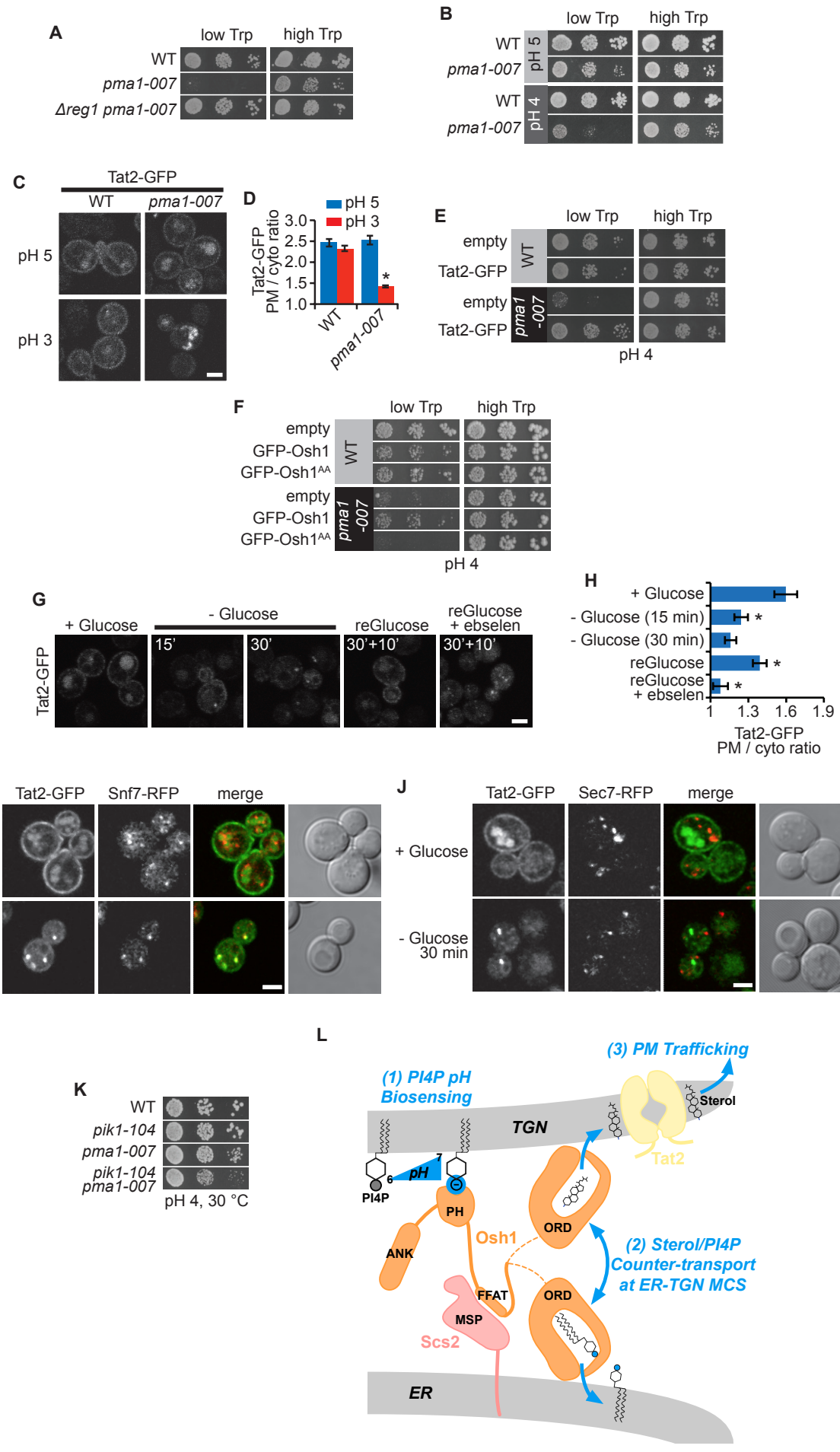
A
low Trp
high Trp
WT
pma1-007
Δreg1 pma1-007
B
low Trp
high Trp
WT
pma1-007
pH 5
WT
pma1-007
pH 4
C
Tat2-GFP
WT
pma1-007
pH 5
pH 3
D
pH 5
pH 3
Tat2-GFP PM / cyto ratio
3.0
2.5
2.0
1.5
1.0
*
WT
pma1-007
E
low Trp
high Trp
empty
Tat2-GFP
WT
empty
Tat2-GFP
pma1-007
pH 4
F
low Trp
high Trp
empty
GFP-Osh1
GFP-Osh1AA
WT
empty
GFP-Osh1
GFP-Osh1AA
pma1-007
pH 4
G
+ Glucose
- Glucose
reGlucose
reGlucose + ebselen
Tat2-GFP
15'
30'
30'+10'
30'+10'
H
+ Glucose
- Glucose (15 min)
- Glucose (30 min)
reGlucose
reGlucose + ebselen
*
*
*
1
1.3
1.6
1.9
Tat2-GFP PM / cyto ratio
I
Tat2-GFP
Snf7-RFP
merge
+ Glucose
- Glucose 30 min
J
Tat2-GFP
Sec7-RFP
merge
+ Glucose
- Glucose 30 min
K
WT
pik1-104
pma1-007
pik1-104 pma1-007
pH 4, 30 °C
L
(1) PI4P pH Biosensing
(3) PM Trafficking
TGN
Sterol
Tat2
pH
7
6
PI4P
PH
ANK
Osh1
ORD
(2) Sterol/PI4P Counter-transport at ER-TGN MCS
FFAT
MSP
Scs2
ORD
ER

Figure 1

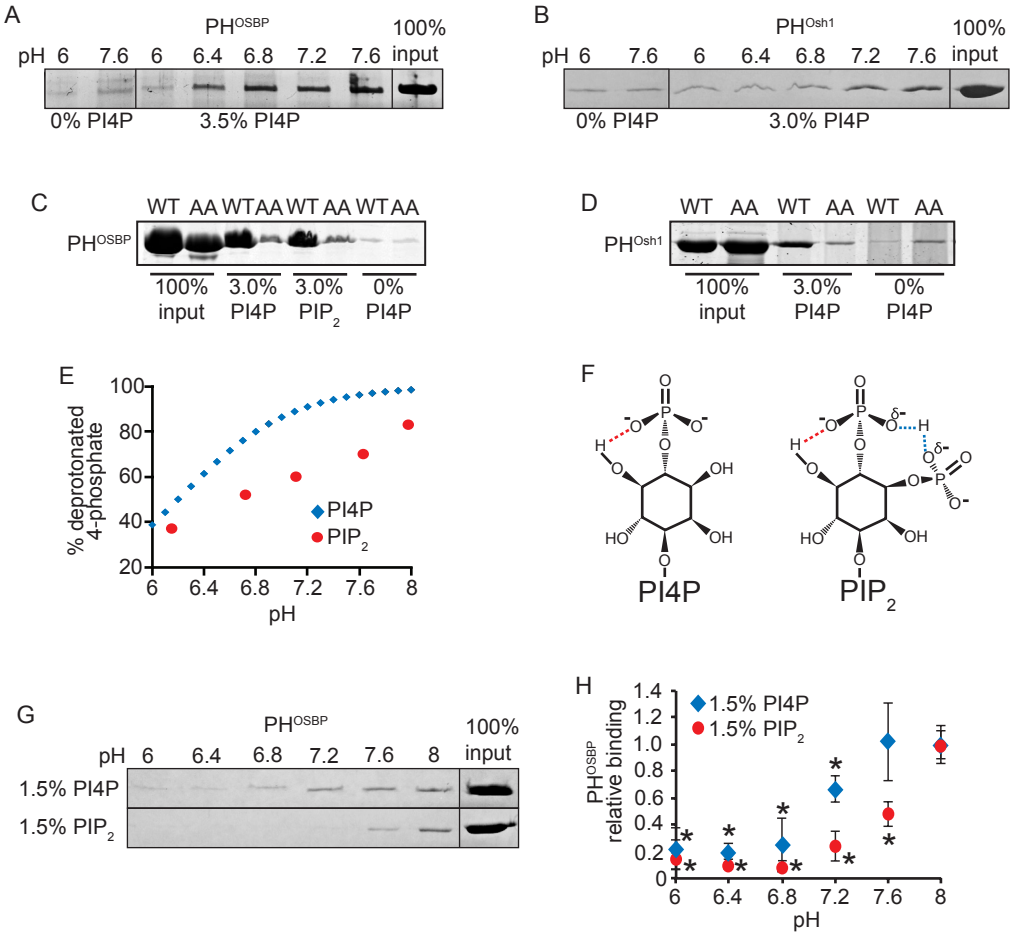
A
PHOSBP
100% input
pH 6 7.6 6 6.4 6.8 7.2 7.6
0% PI4P
3.5% PI4P
B
PHOsh1
100% input
pH 6 7.6 6 6.4 6.8 7.2 7.6
0% PI4P
3.0% PI4P
C
WT AA WT AA WT AA WT AA
PHOSBP
100% input
3.0% PI4P
3.0% PIP2
0% PI4P
D
WT AA WT AA WT AA
PHOsh1
100% input
3.0% PI4P
0% PI4P
E
% deprotonated 4-phosphate
100
80
60
40
20
6 6.4 6.8 7.2 7.6 8
pH
PI4P
PIP2
F
PI4P
PIP2
G
PHOSBP
100% input
pH 6 6.4 6.8 7.2 7.6 8
1.5% PI4P
1.5% PIP2
H
PHOSBP relative binding
1.5% PI4P
1.5% PIP2
1.4
1.2
1.0
0.8
0.6
0.4
0.2
0
6 6.4 6.8 7.2 7.6 8
pH

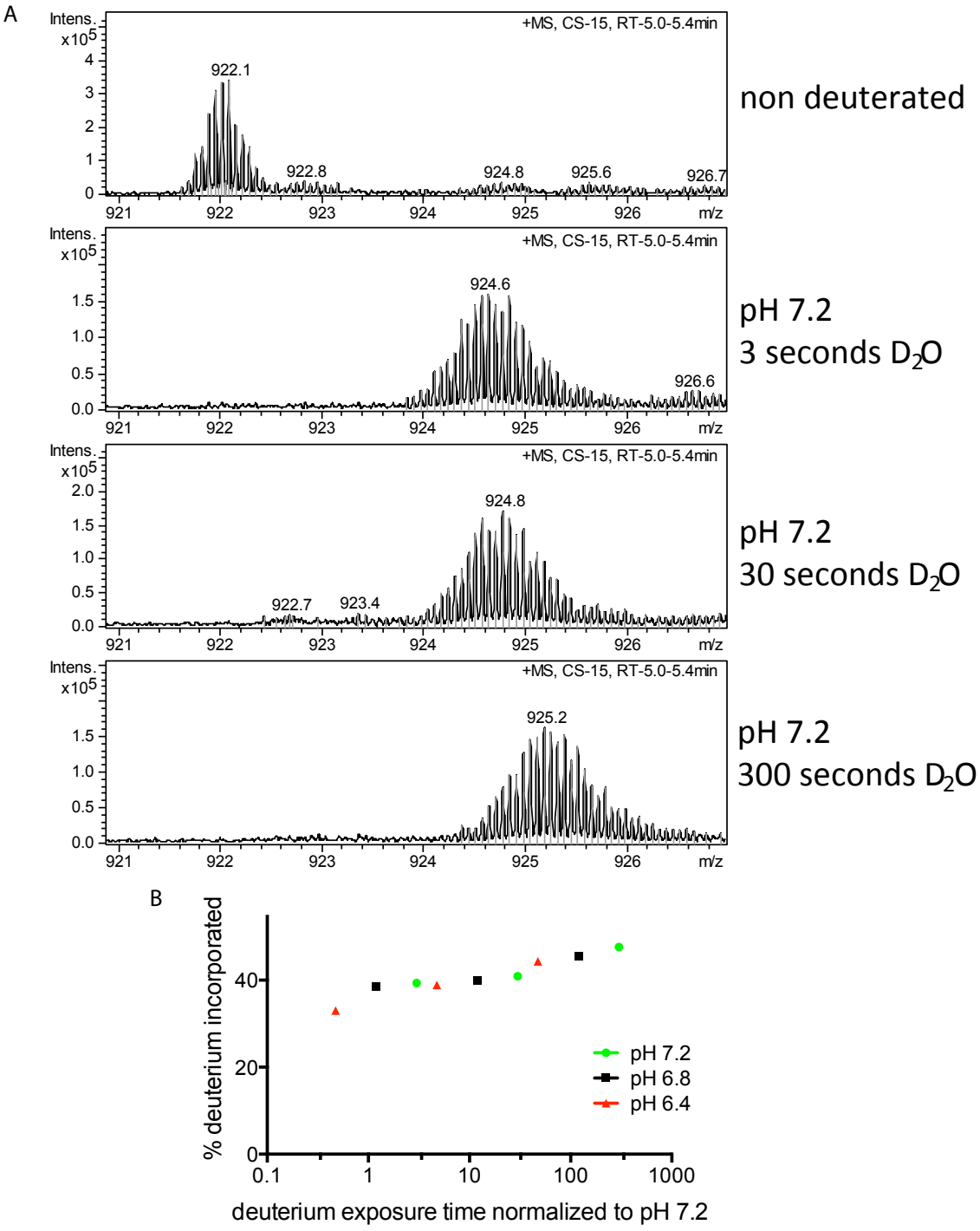

Figure S1. Related to Figure 1. Hydrogen deuterium exchange mass spectrometry of intact OSBP PH domain at different pH values. (A) Intact mass spectrometry of OSBP PH domain is shown in the absence of deuterium, as well as after 3, 30, and 300 seconds of D2O exposure at pH-7.2. Incorporation of amide hydrogens causes the increase in mass seen across the spectrum. (B) The deuterium incorporation values for the OSBP PH domain at three different pHs (6.4,6.8, and 7.2) and at three different time points (3, 30, and 300 seconds) are graphed. For experiments performed at pH-6.4 and pH-6.8 the deuterium incorporation values were normalized to deuterium incorporation at pH-7.2. These deuterium incorporation values are what would be expected for a protein that had minimal conformational changes upon shifting pH. All experiments were repeated as independent triplicates (n=3). For all data the error bars (S.D.) are smaller than the size of the point.

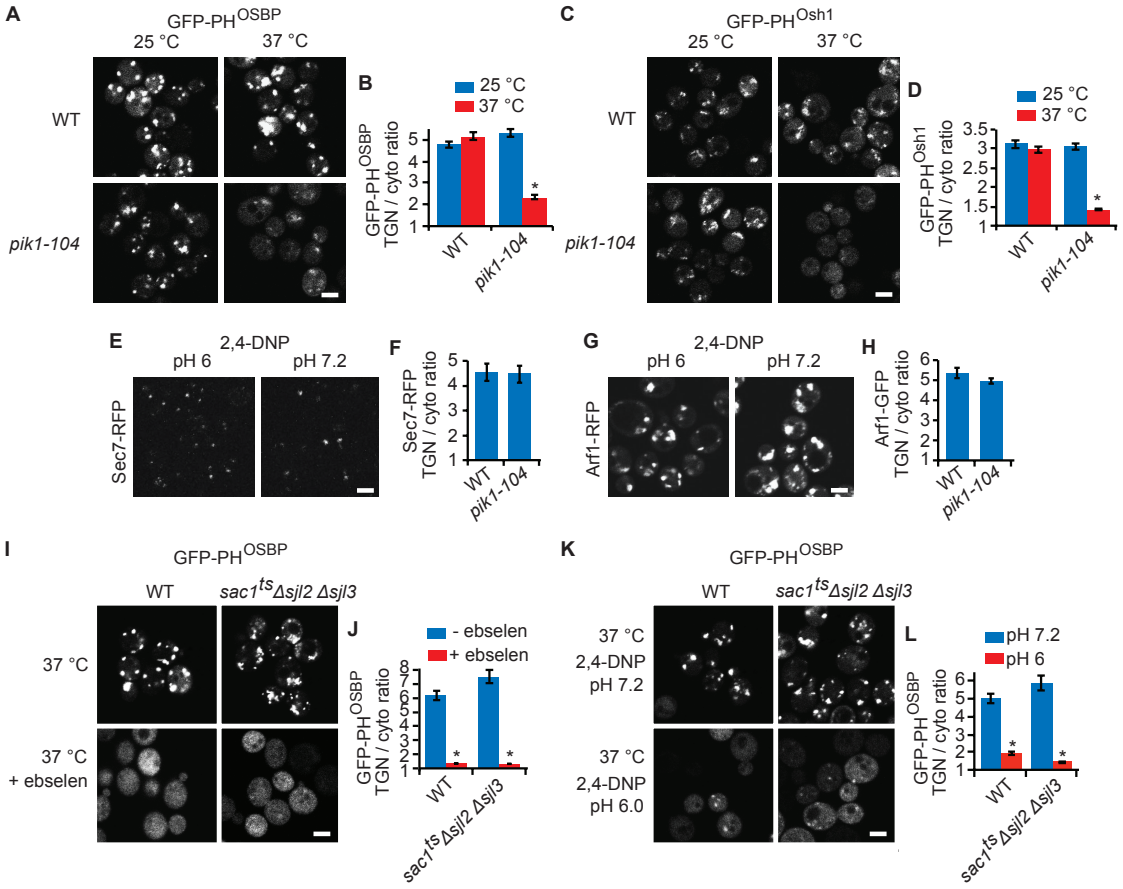

Figure S2. Related to Figure 2. pH_C dependent binding of PH domains to the TGN is independent of general effects on the TGN and turnover of PI4P. (A-D) Confocal micrographs and quantification of WT and *pik1-104* temperature sensitive mutants showing the delocalization of GFP-PH^{OSBP} and GFP-PH^{Osh1} from the TGN in the *pik1-104* mutant when incubated at 37˚C for 1 hour (*, versus 25˚C, P < 0.0001). (E-H) Confocal micrographs and quantification of yeast showing no effect on the TGN localization of Sec7-RFP and Arf1-GFP 10 min after incubation with 2 mM 2,4-DNP buffered at pH 7.2 versus 6. (I,J) Confocal micrographs and quantification of WT and *sac1^{ts} Δsjl2 Δsjl3* triple phosphoinositide polyphosphatase temperature sensitive mutants showing the delocalization of GFP-PH^{OSBP} from the TGN after pre-incubation at 37 °C for 40 min and then addition of 100 µM ebselen for 5 min (*, versus -ebselen, P < 0.0001). (K,L) Confocal micrographs and quantification of WT and *sac1^{ts} Δsjl2 Δsjl3* triple mutants showing the delocalization of GFP-PH^{OSBP} from the TGN after pre-incubation at 37 °C for 40 min and then incubation with 2,4-DNP buffered at pH 6, but not pH 7.2, for 10 min (*, versus pH 7.2, P < 0.0001). Scale bars, 2 µm. WT, wild type. Cyto, cytoplasmic. Error bars indicate SEM.

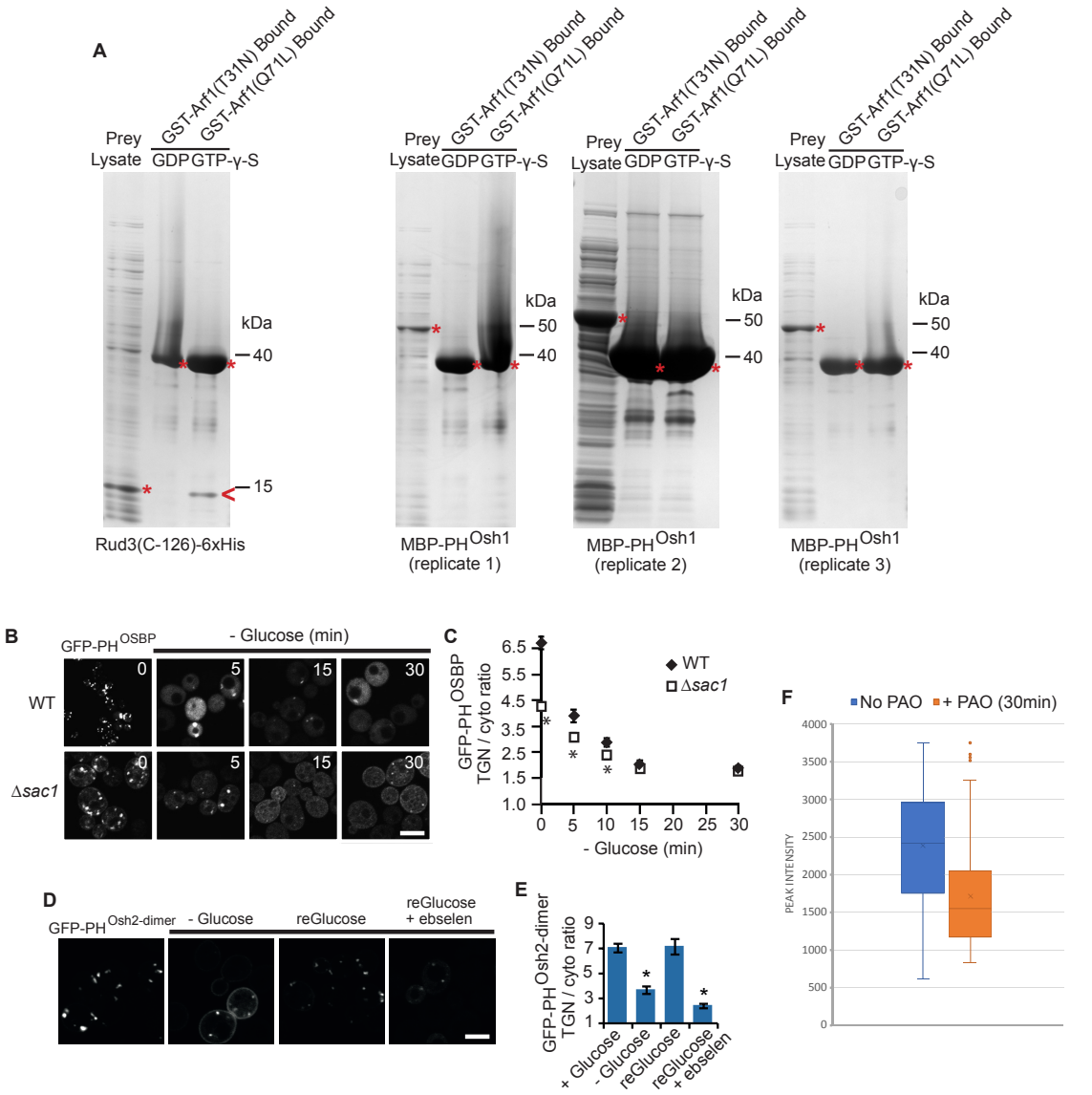

Figure S3. Related to Figure 3. Glucose dependent binding of PH domains to the TGN is independent of their binding to Arf1 and PI4P turnover, but is dependent on pH_C. (A) In vitro Arf1 binding assay. The indicated form of GST-Arf1 (bait) and either Rud3(C-126)-6xHis (postive control) or MBP-PH^{Osh1} (prey) were expressed separately in *E. coli*, and after cell lysis, loaded with the indicated nucleotide. Bait and prey lysates were mixed 1:1 and isolated on glutathione Sepharose Beads. Bound proteins were analysed by gel electrophoresis and coomassie stain. * indicates prey protein in the prey lysate or bait protein in bound fraction. <, prey protein in bound fraction. Rud3 shows a specific interaction with constitutively active Arf1(Q71L) but not inactive Arf1(T31N). No binding of MBP-Osh1 to either Arf1 form was detected in three replicates. (B,C) Confocal micrographs and quantification of WT and *Δsac1* mutants showing the delocalization of GFP-PH^{OSBP} from the TGN when incubated in medium lacking glucose for the indicated time (*, versus WT, $P < 0.05$). (D,E) Confocal micrographs and quantification of yeast showing the localization of GFP-$PH^{Osh2\text{-}dimer}$ after 15 min incubation in medium lacking glucose (- Glucose) and then 5 min after re-addition of glucose (reGlucose) or glucose with 100 µM ebselen (reGlucose + ebselen) to the medium (*, versus + Glucose, $P < 0.0001$). (F) Boxplot of quantification of the TGN localization of Sec7-RFP after 60min of glucose starvation either in the presence or absence of PAO (PAO added after 30min glucose starvation; peak pixel intensity plotted for all detectable TGN localizations; $P < 2e\text{-}16$). Scale bars, 2 µm. WT, wild type. Cyto, cytoplasmic. Error bars in C and E indicate SEM.

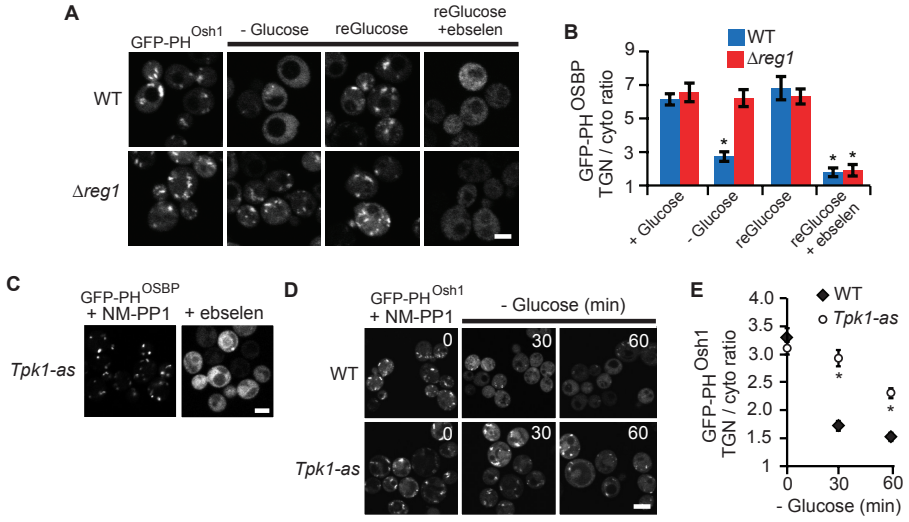

Figure S4. Related to Figure 4. Glucose dependent binding of PH domains to the late-Golgi is dependent on Reg1 and Protein Kinase A regulating pH_C. (A,B) Confocal micrographs and quantification of GFP-PH^{Osh1} localization in WT versus Δ*reg1* mutants showing the effects of 15 min incubation in medium lacking glucose (- Glucose) and then 5 min after re-addition of glucose (reGlucose) or glucose with 100 μM ebselen (+ ebselen) to the medium (*, versus + Glucose, P < 0.0001). Scale bar, 2 μm. . (C) Confocal micrographs showing the localization of GFP-PH^{OSBP} in *Tpk1-as* mutants treated with 1NM-PP1 after addition of 100 μM ebselen. (D, E) Confocal micrographs and quantification of GFP-PH^{Osh1} in WT versus *Tpk1-as* mutants treated with 1NM-PP1 and then incubated in medium lacking glucose (- Glucose) for the indicated time (min) (*, versus WT, P < 0.0001). Scale bar, 4 μm. WT, wild type. Cyto, cytoplasmic. Error bars indicate SEM.

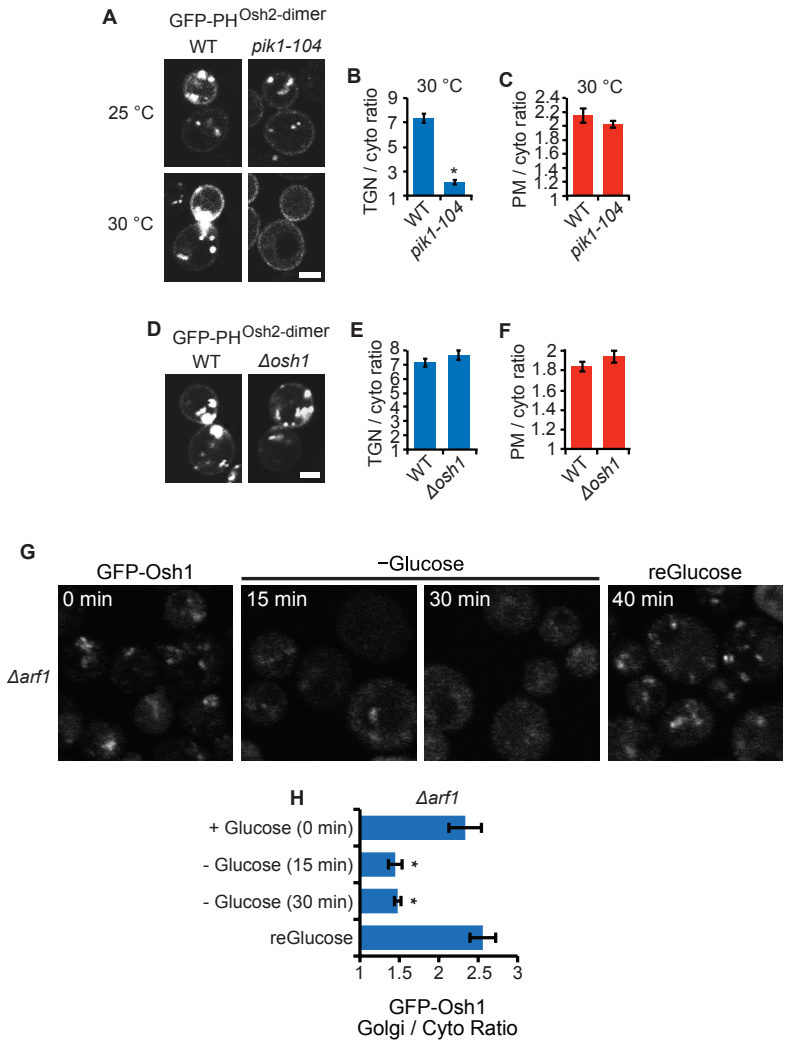

Figure S5. Related to Figure 5. (A) Confocal micrographs of WT and *pik1-104* temperature sensitive mutants showing the delocalization of GFP-PH$^{Osh2\text{-}dimer}$ from the TGN after incubation at the semi-permissive temperature of 30 °C for 1 hour. (B,C) Quantification of TGN and plasma membrane (PM) localization for GFP-PH$^{Osh2\text{-}dimer}$ in (A) (*, versus WT, P < 0.0001). (D) Confocal micrographs and quantification of WT and *Δosh1* mutants showing no difference in the Golgi and PM localization of GFP-PH$^{Osh2\text{-}dimer}$. (E,F) Quantification of TGN and plasma membrane (PM) localization for GFP-PH$^{Osh2\text{-}dimer}$ in (D) (*, versus WT, P < 0.0001). (G,H) Glucose starvation of arf1 yeast expressing GFP-Osh1 and quantitation of Osh1 TGN localization (*, vs 0 min, P < 0.001). Scale bars, 2 μm. WT, wild type. Cyto, cytoplasmic. Error bars indicate SEM.

Supplemental Table 1

Click here to access/download

Supplemental Videos and Spreadsheets

Table S1.xlsx

Supplemental Table 2

Click here to access/download

Supplemental Videos and Spreadsheets

Table S2.xlsx

Supplemental Table 3

Click here to access/download

Supplemental Videos and Spreadsheets

Table S3.xlsx